NATIONAL AERONAUTICS AND SPACE ADMINISTRATION

Technical Report No. 32-808

An Experimental and Analytical Investigation of Concentration Ratio Distributions in a Binary Compressible Vortex Flow

Thomas J. Pivirotto

JET PROPULSION LABORATORY
CALIFORNIA INSTITUTE OF TECHNOLOGY
PASADENA, CALIFORNIA

March 15, 1966

NATIONAL AERONAUTICS AND SPACE ADMINISTRATION

Technical Report No. 32-808

An Experimental and Analytical Investigation of Concentration Ratio Distributions in a Binary Compressible Vortex Flow

Thomas J. Pivirotto

D. R. Bartz, Manager
Research and Advanced Concepts Section

JET PROPULSION LABORATORY
CALIFORNIA INSTITUTE OF TECHNOLOGY
PASADENA, CALIFORNIA

March 15, 1966

Prepared Under Contract No. NAS 7-100
National Aeronautics & Space Administration

CONTENTS

FIGURES

FIGURES (Cont'd)

TABLE

ABSTRACT

A scheme for containing fissionable material in the gas phase in a gaseous-core, nuclear-reactor propulsion system is considered. The results of a referenced analysis of this concept indicate that a rotating annular cloud of highly concentrated fuel gas can be retained in a steady, two-dimensional, potential vortex flow.

The primary objective was to experimentally determine whether a real vortex flow can sustain an annular cloud of a high-molecular-weight gas at room temperature and to determine analytically and experimentally how this cloud is influenced by several of the flow parameters.

Qualitative agreement between the theoretical radial distributions of the heavy to light gas mass density ratio and the measured distributions was found. However, the experimentally determined distributions were found to vary significantly and monotonically from one axial plane to the next, being radially more uniform near the end wall not containing the exit orifice and displaying a definite peak near the opposite end of the vortex tube. In addition, the maximum enrichment factor was found experimentally to increase as the heavy gas mass flow rate was decreased at each of three hydrogen mass flow rates tested. This behavior of the maximum enrichment factor was also found for the analytical model. From the analysis based on a two-dimensional (no axial velocities) potential vortex flow, a critical light gas mass flow rate, with respect to achieving large maximum enrichment factors, was found. This means that if, for any given set of conditions, the actual radial mass flow rate is greater than this critical rate the maximum enrichment factor will be modest, whereas, if the mass flow rate is reduced below the critical rate, the maximum enrichment factor becomes very large indeed.

I. INTRODUCTION

In order to take full advantage of the inherent potential of nuclear energy for rocket propulsion, a means must be found to circumvent the constraints imposed on system performance by the temperature limitations of solid-fuel elements. A possible scheme to accomplish this is one in which a mixture of very-high-temperature, gaseous, fissioning fuel and a gaseous propellant are contained in a chamber in such a way that the energy can be transferred directly to the propellant by particle collision and/or radiation absorption, thereby eliminating the necessity for solid heat-transfer surfaces that are temperature-limited. Because of economic, biological, and performance considerations, it would be essential, however, to separate most of the fuel from the hot propellant before the propellant is expelled.

One such scheme, a gaseous-vortex reactor, is partially analyzed in Ref. 1 and is shown schematically in Fig. 1.

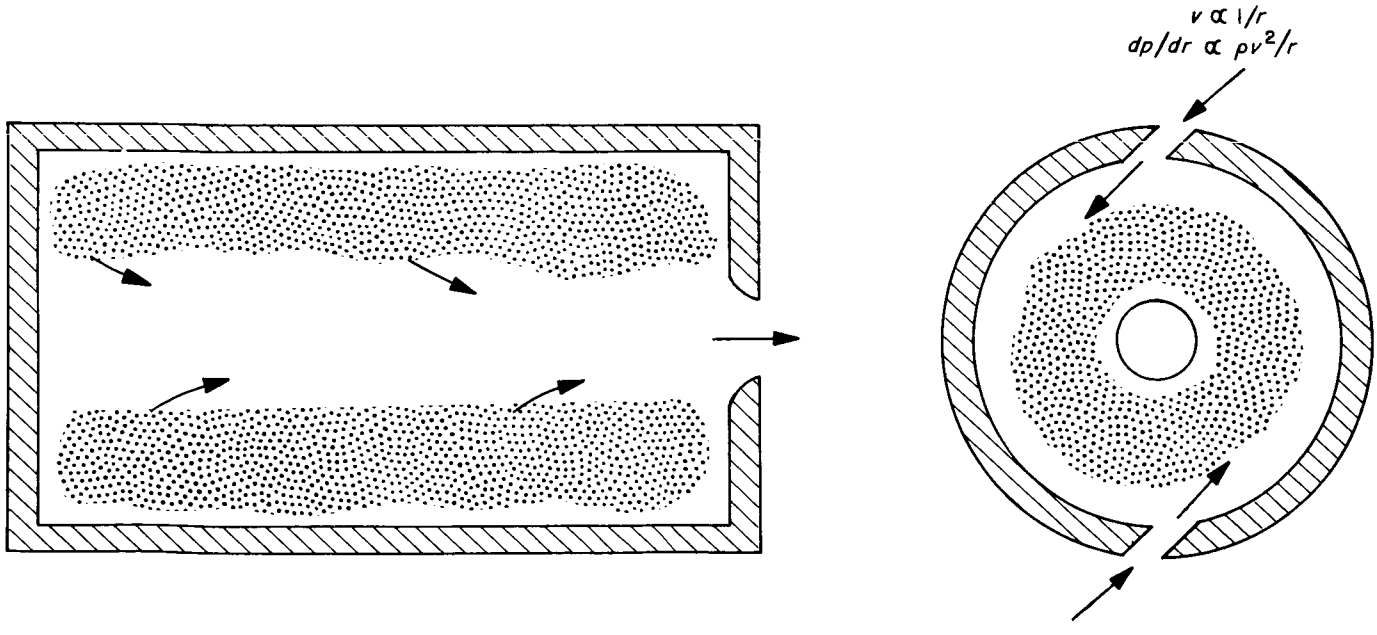

Fig. 1. Vortex separation device

The gaseous-vortex reactor concept takes advantage of the strong radial pressure gradient generated by a vortex-type flow to induce diffusion between the propellant gas, of low molecular weight, and the fuel gas, of much higher molecular weight. Theoretically, the results of this binary diffusion phenomenon would be a low concentration of fuel gas near the cylindrical wall and near the vortex centerline and a high concentration within an annular region of small radial increment. Conceptually, the propellant gas, which is injected tangentially into the vortex tube at the cylindrical wall, migrates radially inward through the hot, dense, annular cloud of fissioning fuel, is heated by attenuating the fission fragments, and then flows axially out through a hole in the center of one end wall.

In the analysis of Ref. 1 the existence of an inviscid, two-dimensional vortex and a laminar diffusion process was assumed. However, it has been shown experimentally in Refs. 2 and 3 that in practice this type of flow is three-dimensional. A significant effect of these axial velocities, induced by the end-wall boundary layers, is to reduce the effective radial mass flow rate. In addition, the fact that this type of flow is turbulent has been inferred from end-wall pressure measurements (Refs. 4, 5) and measured with a hot wire (Ref. 2). It is also well known that the radial distribution of tangential velocity in these real flows is not described very accurately by a potential function.

In Ref. 4, the radial distribution of a fuel-simulating heavy gas was measured in a real binary vortex flow, and it was found that a cloud did in fact develop, and at approximately the radius predicted by the analysis of Ref. 1. However, the cloud was not very dense and the measurements were limited to one axial plane, essentially to one light gas mass flow rate, and to one pair of gases. Consequently, additional experimental and analytical work was needed to further help clarify the characteristics of this type of binary flow and to help determine whether, in fact, the concept of Ref. 1 was realizable.

In an effort to obtain further insight into the effects of a rotating flow on binary mixtures, an experimental investigation was made of the heavy to light gas mass density ratio occurring at various axial and radial locations in the vortex tube. Special emphasis was placed on the effects of mass flow rate, molecular weight, and method of heavy gas injection.

In order to compare these experimental results, which were obtained with room-temperature gases, with an appropriate theory, the analytical model used in Ref. 1 was adopted and modified accordingly. Since the actual radial mass flow rate of light gas $\dot{m}_L$ in any given vortex flow is unknown, this flow rate was treated as a parameter, and the effect of this parameter on the radial distribution of the heavy to light gas mass density ratio ρ_H/ρ_L was determined from this modified analytical model. By comparing these results with experiments, an estimate of the actual light gas mass flow rate occurring in the experiments was obtained. In addition, this modified model was used to study the maximum enrichment factor $(\rho_H/\rho_L)_{max}/(\rho_H/\rho_L)_\infty$ and the way in which this factor was influenced by variables such as light gas mass flow rate and the ratio of heavy to light gas mass flow rate $\dot{m}_H/\dot{m}_L$.

The static pressure on the closed end wall of the vortex tube was measured for both hydrogen and nitrogen gas flows, and the differences were noted. Also, from similar measurements with nitrogen, the radial distribution of the diffusion-causing radial pressure gradient $d \ln p/dr$ was determined as a function of mass flow rate and exit-hole diameter.

Since the density ratio measurements required the introduction of a probe into the binary flow, the effects of this type of probe on the end-wall pressure distribution was determined. The type of probe considered consisted of a plain cylindrical rod extending completely across the vortex tube along a diameter, and end-wall pressure measurements were made for various probe diameters, probe axial positions, and nitrogen mass flow rates.

II. EXPERIMENTAL EQUIPMENT AND TECHNIQUES

A. Vortex Tube

Two basic vortex tubes were used for these experiments, Model A and Model B.

Model A, which was used for most experiments, consisted of two concentric cylindrical steel tubes held together at both ends by flanges onto which the end walls were bolted (Fig. 2). The annular space between the tubes served as a manifold, which supplied the high-pressure gas or binary gas mixture to each of 804 driving jet tubes. These tubes were fabricated of stainless-steel tubing of 0.062-in. OD and 0.007-in. ID, cut into 0.90-in. lengths and cemented into holes drilled through the wall of the inner tube. The overall effect of this arrangement was to have 0.007-in.-D jets arranged in a helix and tangent to a circle whose diameter was 92% of the inner tube ID. The helix contained six equally spaced jets per cycle and had a pitch of 0.180 in. This pattern of jets covered the entire inner cylindrical surface of the vortex tube, which was 24.14 in. long and 4.50 in. in diameter.

For all experiments, the fluid from the vortex tube was discharged into the atmosphere through an orifice at the center of one end wall. Since the pressure level near the vortex centerline was found to be always below one atmosphere, a center plug was used to prevent the external fluid from being drawn into the vortex during the separation experiments. Such a recirculation would cause deceleration of the rotating flow near the centerline and, what is perhaps more significant, contamination of the binary mixture. For each mass flow rate of hydrogen investigated, the center plug was moved along the vortex

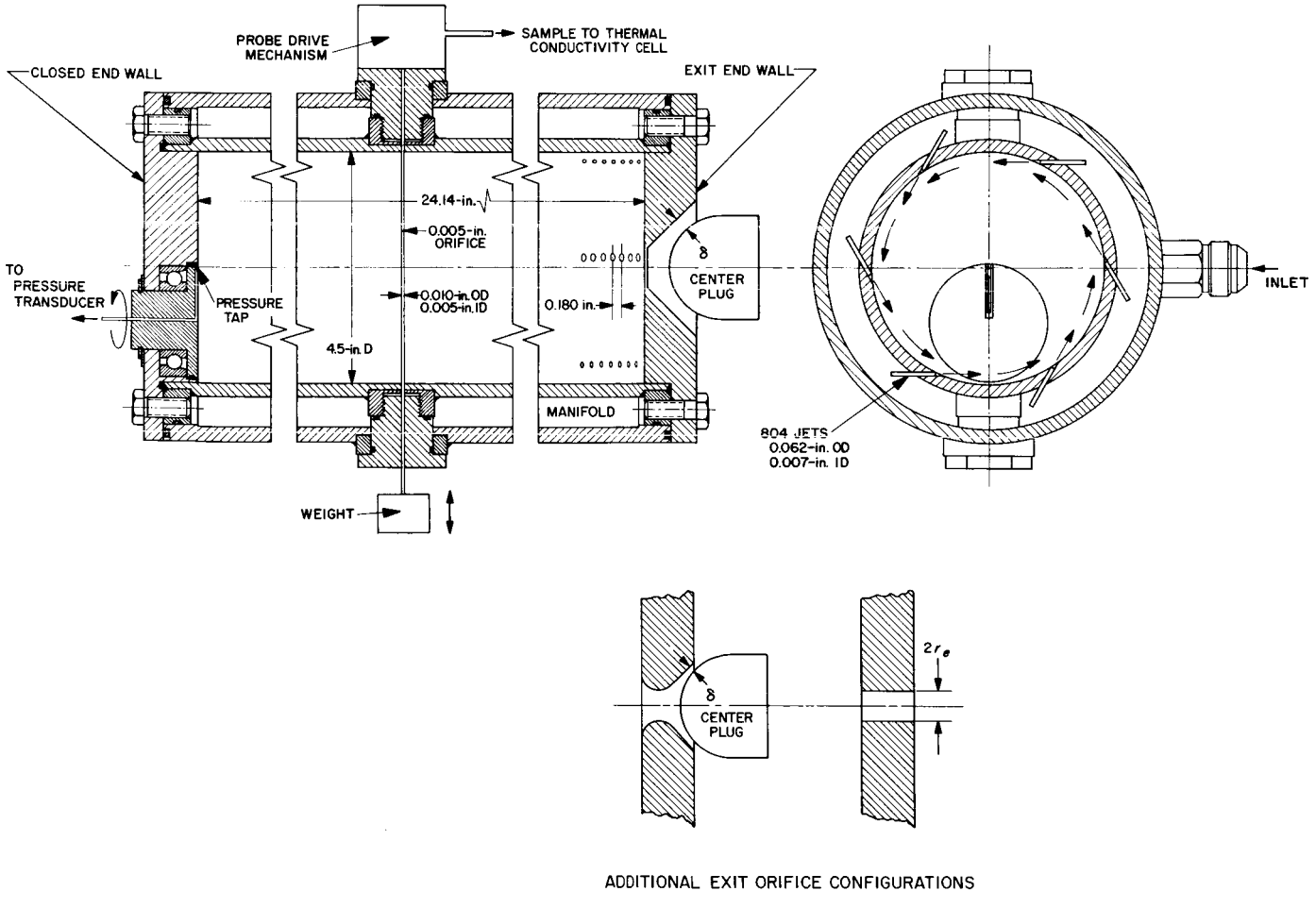

Fig. 2. Experimental vortex tube

tube centerline until the pressure at the center of the closed end wall was minimized. It was found, by sampling and analyzing the flow near the centerline, that this arbitrary criterion was sufficient to insure that no air was being recirculated. It is also believed that this criterion ensured that the flow was not being excessively restricted by the center plug.

Pressure fluctuations measured at the periphery of the closed end wall by a transducer were reduced from approximately 1% to 0.1% by contouring the exit orifice inlet as shown in Fig. 2. However, this exit orifice configuration change had no measurable effect on the density ratio distributions. For the nitrogen experiments from which the radial distribution of the radial pressure gradient was determined, cylindrical orifices of various diameters were used, as shown in Fig. 2.

Model B, used for the probe effect experiments, was made of Lucite and had an internal diameter of 3.0 in. and a length of 16.0 in. The fluid, dry nitrogen was injected into the tube through a single longitudinal row of 80 equally spaced holes drilled through the tube wall. Each jet was 0.040 in. in diameter and approximately tangent to the inner surface of the vortex tube. The fluid was exhausted to the atmosphere through a hole at the center of one end wall.

B. Fluid Supply Systems

The hydrogen and nitrogen mass flow rates were measured with a choked venturi located upstream of the vortex tube manifold, and a rotameter was used to measure the mass flow rate of the heavy gas during the diffusion experiments. For most experiments this heavy gas was injected into the hydrogen through the throat tap of a second venturi located in the hydrogen gas supply line downstream of the choked venturi and 16 in. upstream of the vortex tube manifold. For several experiments the heavy gas was injected directly into the vortex tube at the center of the closed end wall. For this purpose an injector (Fig. 3), installed in the end wall, imparted a swirl to the heavy gas to minimize its effect on the hydrogen vortex. For several such experiments, a deflector

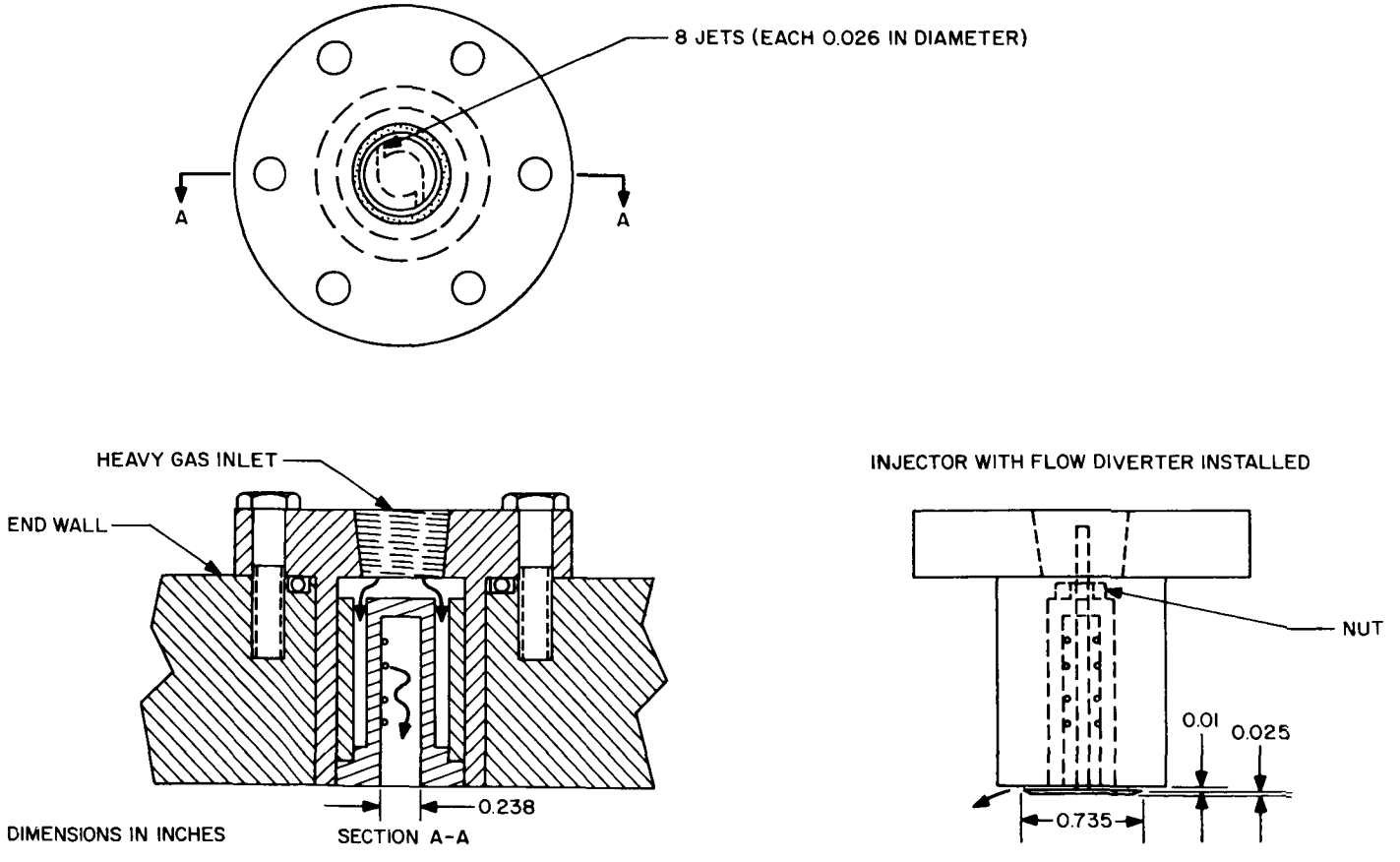

Fig. 3. Heavy gas injector

plate was used to reduce the axial velocity component of the heavy gas.

C. Pressure and Temperature Measurements

A pitot tube and a bare-wire thermocouple were used to measure the fluid stagnation pressure and temperature 15 in. upstream of the choked venturi. The manifold pressure and temperature were also recorded for each experiment. In addition, the static pressure at the vortex tube cylindrical wall, measured at the closed end of the tube, was monitored and held constant during each run.

The radial static-pressure distribution on the closed end wall of Model A was obtained with a pressure tap located in a disk which was built into the closed end wall and which could be rotated as shown in Fig. 2. The pressure tap had a diameter of 0.010 in. and was approximately 0.020 in. deep. This disk had its axis displaced 1.063 in. from the vortex tube centerline and was flush with the end-wall inner surface. By rotating this disk, the static pressure at any radial position from the centerline to a point 0.127 in. from the vortex tube's cylindrical surface could be determined. The radial position of the pressure tap was indicated remotely by a signal from a selsyn motor that was geared to the disk shaft. This radial position r is equal to the cord distance between the vortex tube centerline and the tap position, which was 0.061 in. from the disk periphery, or

$$r = 2a \sin \frac{\theta}{2} \tag{1}$$

The constant a is the fixed distance between the disk center and the pressure tap location, or 1.063 in., and θ is the angular orientation of the disk. Since the selsyn output is proportional to sin ϕ, where ϕ is the angular orientation of the selsyn armature, r was directly proportional to the selsyn output because a 2-to-1 gear ratio between selsyn and disk was used, making $\phi = \theta/2$. This signal was put directly on the x-axis of an x-y plotter and the pressure transducer signal on the y-axis. In this way, a trace of $p = p(r)$ was obtained directly.

The radial clearance between the disk and the mating hole was 0.0002 in., in order to minimize the amount of fluid trapped in the resulting circumferential gap. This fluid would be driven radially inward by the external radial pressure gradient and would erupt from the gap near the vortex tube centerline, disturbing the end-wall boundary layer. The fluid was prevented from leaking out through this gap by an O-ring located 0.050 in. beneath the inner surface of the end wall.

The end wall containing the exit hole was provided with five pressure taps, each one 0.020 in. in diameter, located at discrete radial positions. These pressure taps were connected to a pneumatic switch and the pressure was measured by a transducer. This same arrangement was used to measure the radial pressure distribution on the closed end wall of Model B.

D. Mass Density Ratio Measurements

In order to measure the radial distribution of the ratio of heavy to light gas mass density ρ_H/ρ_L, a sampling probe was developed that utilized a stainless steel tube with a 0.010-in. OD and a 0.005-in. ID, located diametrically across the vortex tube (Fig. 2). The probe was held in position under tension by a 1.97-lb weight, and could be installed at five discrete axial positions. The principal advantage of this type of sampling probe is that the disturbance of the flow by the probe does not vary as the radial position of the probe is changed. A 0.005-in.-D hole was drilled through the tube wall to provide a means of obtaining samples. With a vacuum pump, the sample was extracted continuously from the binary vortex flow through a thermal conductivity cell, Model 30-TH, made by the Gow-Mac Instrument Co. of Madison, New Jersey. Since the pressure at the probe inlet varied considerably with radial position, a system was provided for bleeding part of the sample off at a point upstream of the thermal conductivity cell. By varying the bleed mass flow rate as the radial survey was made, the pressure and flow rate of the sample to be analyzed in the thermal conductivity cell could be held very closely to predetermined values. The flow rate of the sample passing through the thermal conductivity cell was monitored with a rotameter and the pressure with a transducer. Pure hydrogen was withdrawn from the supply line and bled through the reference side of the thermal conductivity cell at a pressure and mass flow rate approximately equal to that of the test sample withdrawn from the vortex tube. The signal from the thermal conductivity cell bridge, which was proportional to the difference in thermal conductivity between pure hydrogen and the hydrogen–heavy gas mixture, was used to drive the y-axis of an x-y plotter. The radial position of the probe orifice was sensed by a linear potentiometer and this signal was used to drive the x-axis. Since it was determined by calibration that, for most operating conditions, the thermal conductivity cell output was linearly proportional to the ratio of heavy to light gas mass density in the sample, a plot of density ratio vs radius was obtained directly during an experiment. For conditions at which it was found that the calibration was not linear

(high-density ratios), the density ratio measurements were modified by applying corrections obtained from the calibration curves. In addition, the data were corrected for electrical drift by obtaining the cell output before and after each run while pure hydrogen was flowing through the vortex tube.

III. RESULTS AND DISCUSSION

A. Analytical Development

The effect of fuel and propellant mass flow rate on the density ratio ρ_H/ρ_L was determined from an analysis of the flow model proposed in Ref. 1.

1. Radial Density Ratio Distributions

The radial mass flow at any given radius can be different from that at the cylindrical wall because of the axial diversion of the flow; consequently it is of interest to determine analytically the specific effect of the radial mass flow rate on the radial distribution of the density ratio ρ_H/ρ_L. To accomplish this, the basic model used in Ref. 1 was adopted. This model can be described as an axisymmetric, steady, compressible flow of a mixture of two inviscid gases differing in molecular weight, with a zero axial velocity in the annular region of interest and an inward radial velocity that is everywhere much smaller than the tangential velocity. In addition, the diffusion process is assumed to be laminar, with no thermal or body force diffusion and no chemical reactions.

Since no heat release occurred in the diffusion experiments performed, the term describing an energy release has been excluded from the problem. It was shown in Ref. 1 that, for all heating rates lower than a specified critical rate, the radial distributions of ρ_H/ρ_L have the same general shape and that heating rates lower than the critical rate are of interest for a propulsion device. The problem is now considerably simplified, since, with the assumption of no heat generation, the energy equation is uncoupled from the rest of the equations and becomes tractable. The assumption of an axisymmetric two-dimensional flow implies a constant radial mass flow rate in the region of interest, a contradiction of the experimental results. It is assumed here, however, that the primary effect on the density ratio distribution is caused by the reduced level of mass flow rate and not by the variation of mass flow rate with radius. The assumption that the flow is inviscid implies that the tangential velocity is a function of the reciprocal radius only. In a real flow the tangential velocity also depends on the radial mass flow rate and probably on its distribution as well. The tangential velocity level in the vortex flow is determined by the parameter Γ, a free parameter in this analysis, equal to vr. Notice that, by the assumption of the value for Γ in these computations, the radial pressure gradient $d \ln p/dr$ is fixed. This means that the results of this analysis do not depend on pressure level explicitly. In the analysis of Ref. 1 the heavy gas particle density n_H was restricted to levels much lower than that of the light gas n_L. However, in the derivation of the equation used here, this restriction was found unnecessary, and in this way the results herein are somewhat more general, although, of course, they are restricted to flows with no heat generation, as mentioned previously.

With the assumption of no chemical reactions, the heavy gas continuity equation, written in terms of the density ratio ρ_H/ρ_L and the total continuity equation, can be combined and integrated in closed form. This result, together with the radial momentum equation, the integrated tangential momentum and energy equations, and the equation for the binary diffusion coefficient based on rigid elastic spheres, can be combined with the equation for the heavy gas diffusion velocity to form the following ordinary, first-order, nonlinear Riccati-type differential equation:

$$\frac{(a_0 r^2 - a_1)^{1/2}}{a_2} \frac{d\rho_H/\rho_L}{dr} + \left(\frac{\rho_H}{\rho_L}\right)^2 + \left(\frac{a_3}{r(a_0 r^2 - a_1)^{1/2}} + a_4\right)\frac{\rho_H}{\rho_L} + a_5 = 0 \qquad (2)$$

where

$$a_0 = T_\infty$$

$$a_1 = \frac{\left(\frac{\dot{m}_H}{\dot{m}_L} + 1\right)\Gamma^2}{2g_c C_{p_L}\left(1 + \frac{\dot{m}_H}{\dot{m}_L}\frac{C_{p_H}}{C_{p_L}}\right)}$$

$$a_2 = -\dot{m}_L\left[\frac{2\pi}{m_H\left(\frac{m_H}{m_L} + 1\right)k\,g_c}\right]^{1/2}\frac{4(\sigma_{LH})^2}{3\pi}$$

$$a_3 = -\frac{1}{\dot{m}_L}m_L\left(1 - \frac{m_H}{m_L}\right) \times\left[m_H\left(1 + \frac{m_H}{m_L}\right)\frac{2\pi}{k\,g_c}\right]^{1/2}\Gamma^2\frac{3}{8(\sigma_{LH})^2}$$

$$a_4 = \frac{m_H}{m_L} - \frac{\dot{m}_H}{\dot{m}_L}$$

$$a_5 = -\frac{\dot{m}_H}{\dot{m}_L} \times \frac{m_H}{m_L}$$

The Riccati equation cannot, in general, be solved by quadratures, although, with certain restrictions on the coefficients, solutions can be developed by methods presented in Refs. 6 and 7. The coefficients of Eq. (2) appear not to satisfy these restrictions; consequently, solutions were obtained on a digital computer.

For computational purposes, Eq. (2) was normalized with respect to conditions at the radial point at which the density ratio distribution reaches a maximum. This point was found by setting the slope $(d\rho_H/\rho_L)/dr$ equal to zero and solving the resulting fifth order algebraic equation for radius r. It was found that this equation had two real roots, one plus and one minus; two imaginary roots; and a fifth root at infinity. The only physically significant roots are the plus real root and infinity. To prove that the positive real root represents a local maximum, the Riccati equation was differentiated with respect to radius, and the sign of the second derivative was determined and found to be negative for all values of the parameters. Also, since the slope of the radial distribution of the density ratio is zero at infinity, it is clear that the density ratio distribution reaches a local minimum at infinity. Therefore the radial distribution of the density ratio ρ_H/ρ_L has but one maximum, located at

$$r_{\max} = \left(\frac{a_1}{2a_0} + \left\{\left(\frac{a_1}{2a_0}\right)^2 + \frac{1}{a_0}\left[\frac{a_3(\rho_H/\rho_L)_{\max}}{(\rho_H/\rho_L)^2_{\max} + a_4(\rho_H/\rho_L)_{\max} + a_5}\right]^2\right\}^{1/2}\right)^{1/2} \tag{3}$$

and one minimum, located at $r_{\min} = \infty$.

For very large radii, the Riccati equation can be simplified and, with a simple transformation of the independent variable, can be integrated. By this procedure it can be shown that the density ratio ρ_H/ρ_L approaches the ratio of mass flow rates $\dot{m}_H/\dot{m}_L$ as the radius r approaches infinity. These conditions at infinity correspond with conditions in the manifold of an experimental vortex tube for which the heavy and light gases are premixed. This binary diffusion problem requires that two boundary conditions be specified in order to obtain a specific solution. For convenience, these two conditions were taken at $r_{\max}$ and $r_{\min}$ by specifying the maximum density ratio and the ratio of mass flow rates. It can be seen that the maximum density ratio and its radial location cannot both be predicted, even when all other parameters are known. Indeed, the relationship between the maximum density ratio and its radial location can be determined, it is believed, only by experiment.

2. Effect of Mass Flow Rate $\dot{m}_L$ on the Density Ratio Distribution

To illustrate the effect of the light gas mass flow rate $\dot{m}_L$ on the radial distribution of the density ratio ρ_H/ρ_L, Eq. (2) was integrated for several values of $\dot{m}_L$ while the boundary conditions and all other quantities were held constant and approximately equal to those used in an experiment to be discussed subsequently. To maintain a constant circulation while the mass flow rate is varied would require a variable injection configuration in practice. The parametric values are listed in Table 1 and the results of the integration are shown in Fig. 4 as density ratio divided by the density ratio at infinity, which was a boundary condition, plotted against a normalized radius. To normalize r, the radius of the vortex tube, r_w, used in the experiments described in this Report, was chosen arbitrarily. The effect of reducing the light gas mass flow rate is to broaden the distributions and to shift the radius of maximum density ratio to larger radii. These effects can be explained from an investigation of the continuity and diffusion equations for the light and heavy gases.

Table 1. Parametric values for the theoretical computations of Fig. 4

Parameter	Value
C_{p_L}, $\frac{\text{ft-lbf}}{\text{lbm °R}}$	2.638×10^3
C_{p_H}, $\frac{\text{ft-lbf}}{\text{lbm °R}}$	1.230×10^2
$\dot{m}_H$, $\frac{\text{lbm}}{\text{sec-ft}}$	-5.0×10^{-4}, -5.0×10^{-5}, -5.0×10^{-6}, -5.0×10^{-7}, -5.0×10^{-8}
$\dot{m}_L/\dot{m}_H$	18
m_L, $\frac{\text{lbm}}{\text{molecule}}$	7.384×10^{-27}
m_H, $\frac{\text{lbm}}{\text{molecule}}$	3.827×10^{-25}
T_∞, °R	533
$\left(\frac{\rho_H}{\rho_L}\right)_{\max}$	0.085
σ_{LH}, $\frac{\text{ft}}{\text{molecule}}$	1.148×10^{-9}
Γ, $\frac{\text{ft}^2}{\text{sec}}$	62.18

Dividing the integrated heavy gas continuity equation by that for the light gas and noting that there can be no net mass flux by diffusion, the following expression is obtained;

$$\frac{\dot{m}_H}{\dot{m}_L} = \frac{\rho_H}{\rho_L}\left(\frac{u_0 + \bar{u}_H}{u_0 - \frac{\rho_H}{\rho_L}\bar{u}_H}\right) \tag{4}$$

The mass average radial velocity u_0 is approximately proportional to the light gas mass flow rate $\dot{m}_L$ in this problem and inversely proportional to the radius r, while the heavy gas diffusion velocity $\bar{u}_H$, which is relative to u_0, is independent of this mass flow rate and approximately proportional to the radial pressure gradient $d \ln p/dr$. Therefore, for a given flow field and mass flow rate ratio, as was considered in Fig. 4, and at any given large radius, the density ratio must increase as the light gas mass flow rate $\dot{m}_L$ is reduced. This means that as the heavy gas absolute inward radial velocity $(u_0 + \bar{u}_H)$

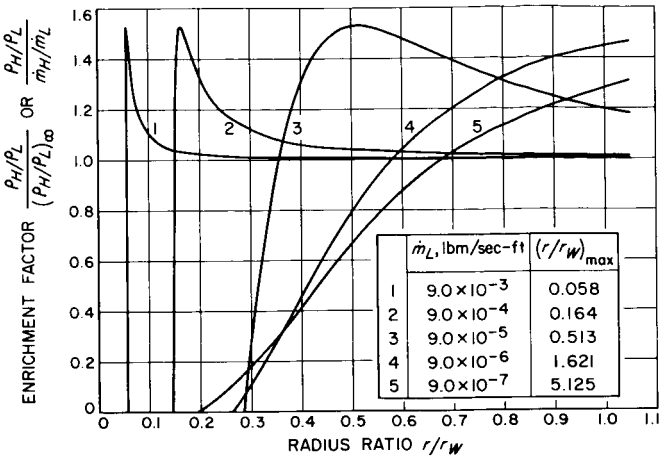

Fig. 4. Theoretical density ratio distributions

decreases, the heavy gas density relative to that of the light gas increases in order to maintain a constant mass flow rate ratio. The inverse is true of the light gas, that is, ρ_L decreases because of diffusion, causing a further increase in ρ_H/ρ_L. Since the maximum density ratio is fixed as a boundary condition in this problem, the distribution reaches this limit at larger radii as the light gas mass flow rate is reduced. Note in Fig. 4 that a ten-fold decrease in light gas mass flow rate causes the radius at which the peak density ratio occurs to increase by approximately a factor of three. Also, at the larger radii the radial pressure gradient changes more slowly with radius, causing a more gradual change in density ratio and hence a broader distribution. At radii less than that of the peak density ratio the density ratio *gradient* is positive and as such decreases the heavy gas diffusion velocity, resulting in a rapidly decreasing density ratio with radius.

3. Maximum Enrichment Factor $(\rho_H/\rho_L)_{\max}/(\rho_H/\rho_L)_\infty$

In the propulsion concept of Ref. 1, one of the requirements of the diffusion process was to produce a very large maximum enrichment factor $(\rho_H/\rho_L)_{\max}/(\rho_H/\rho_L)_\infty$ or the equivalent $(\rho_H/\rho_L)_{\max}/\dot{m}_H/\dot{m}_L$. In fact, in the analysis of Ref. 1, maximum enrichment factors between 5×10^3 and 4×10^4 were assumed. As has been pointed out previously, it is not possible to predict the maximum enrichment factor obtainable under a given set of conditions unless its radial location is first assumed. However, it has been found instructive to determine how this factor is affected by the other parameters for any given value of $r_{\max}$. This has been done by setting the gradient in Eq. (2) equal to zero and solving the resulting algebraic equation for the maximum enrichment factor. A positive

and a negative root are obtained, and by discarding the physically unrealistic negative root the result is:

$$\frac{(\rho_H/\rho_L)_{\max}}{\dot{m}_H/\dot{m}_L} = \frac{b_0}{2} + \left[\left(\frac{b_0}{2}\right)^2 + b_1\right]^{1/2} \qquad (5)$$

where

$$b_0 = \left\{ \frac{3m_L\left(1 - \frac{m_H}{m_L}\right)\left[m_H\left(1 + \frac{m_H}{m_L}\right)\frac{2\pi}{k\,g_c}\right]^{1/2}\Gamma^2}{8(\sigma_{LH})^2\,\dot{m}_L\left(\frac{\dot{m}_H}{\dot{m}_L}\right) r_{\max}\left[T_\infty\, r_{\max}^2 - \frac{(\dot{m}_H/\dot{m}_L + 1)\,\Gamma^2}{2\,g_c\,C_{p_L}\left(1 + \frac{\dot{m}_H}{\dot{m}_L}\frac{C_{p_H}}{C_{p_L}}\right)}\right]^{1/2}} - \frac{m_H/m_L}{\dot{m}_H/\dot{m}_L} + 1 \right\}$$

$$b_1 = \frac{m_H/m_L}{\dot{m}_H/\dot{m}_L} = \frac{\dot{n}_L}{\dot{n}_H}$$

From Eq. (5) the maximum enrichment factor has been computed as a function of the mass flow ratio $\dot{m}_H/\dot{m}_L$ for several light gas flow rates $\dot{m}_L$ and several values of $r_{\max}$. The results shown in Fig. 5 are for a Freon-13–hydrogen mixture; in Fig. 6, for a uranium–hydrogen mixture that is of possible interest in a propulsion device; and in Fig. 7, for a helium–hydrogen mixture that might be of interest in other gas separation applications in which the two species have only a small difference in molecular weight. For these calculations the heavy gas molecular weight m_H was varied, but the heavy gas specific heat C_{p_H} and collision cross section σ_{LH} were not. Instead, the values for C_{p_H} and σ_{LH} given in Table 1 for Freon-13, were used throughout. The values for C_{p_L}, m_L, T_∞, and Γ given in Table 1 were also used in these computations.

The most interesting feature of Figs. 5, 6, and 7 is that there appears to be some critical light gas mass flow rate. When the actual light gas mass flow rate is greater than this critical rate, the maximum enrichment factor is modest and almost independent of mass flow ratio $\dot{m}_H/\dot{m}_L$. But when the light gas mass flow rate is less than this critical rate, the maximum enrichment factor becomes very large and is then approximately proportional to the reciprocal mass flow ratio $(\dot{m}_H/\dot{m}_L)^{-1}$. This means that for high light gas mass flow rates the maximum density ratio $(\rho_H/\rho_L)_{\max}$ varies as the general density level in the vortex varies, while with low light gas mass flow rates the maximum density ratio remains at a high level relative to, and independent of, the initial density ratio $(\rho_H/\rho_L)_\infty$ or $(\dot{m}_H/\dot{m}_L)$. This trend was found for all heavy gases and for all assumed values of the radial location of the maximum enrichment factor $r_{\max}$. However, it must be remembered that $r_{\max}$ may not remain constant as the mass flow rates $\dot{m}_H$ and $\dot{m}_L$ are reduced. For example, in Fig. 5, if the vortex were to be operated at an $\dot{m}_L$ of 5×10^{-5} lbm/sec-ft and if $\dot{m}_H/\dot{m}_L$ were decreased from 10^{-1} to 10^{-2}, the maximum enrichment factor would increase by approximately a factor of 10 if $r_{\max}$ did not change, by more than 10 if $r_{\max}$ decreased, and by less than 10, or would decrease, if $r_{\max}$ increased as $\dot{m}_H/\dot{m}_L$ decreased. Note that in a propulsion device, a decrease in the mass flow ratio $\dot{m}_H/\dot{m}_L$ means a decrease in fuel expenditure per pound of propellant used. However, the fuel mass flow rate cannot be decreased without limit (in the hope of achieving large enrichment factors) since the fuel is consumed at a certain rate and the flow rate must be at least large enough to feed this reaction. The dependence of $r_{\max}$ on the mass flow rates $\dot{m}_H$ and $\dot{m}_L$ must come from experiment.

A second restriction on these parameters, with respect to the gaseous-vortex reactor concept, is that the absolute fuel gas density must satisfy criticality. Estimates of criticality, made in Ref. 1, show that average fuel densities of order 10^{18} particles/cm^3 might be required. If we take as a model the vortex tube used in Ref. 1, Case 3 (p. 61), which was 0.68 in. in diameter, and a flow field of hydrogen–uranium^{235} at a temperature level of 7500°R and a circulation of 62.0 ft^2/sec, and assume a desirable fuel loss rate of 10^{-4} lbm per lbm of hydrogen expended, and an $r_{\max}$ of 0.24 in., Eq. (5) gives a maximum enrichment factor of 3.2 for a propellent mass flow rate of 2×10^{-3} lbm/sec-ft. However, if this mass flow rate is reduced by a factor of two and all other parameters are maintained the same, the maximum enrichment factor jumps to 4.4×10^5. The analysis of Ref. 1 also provides the following expression for the cylindrical wall pressure:

$$p_W \simeq \frac{4.8\,R_L\,T_W\,\bar{\rho}_H}{(\rho_H/\rho_L)_{\max}}$$

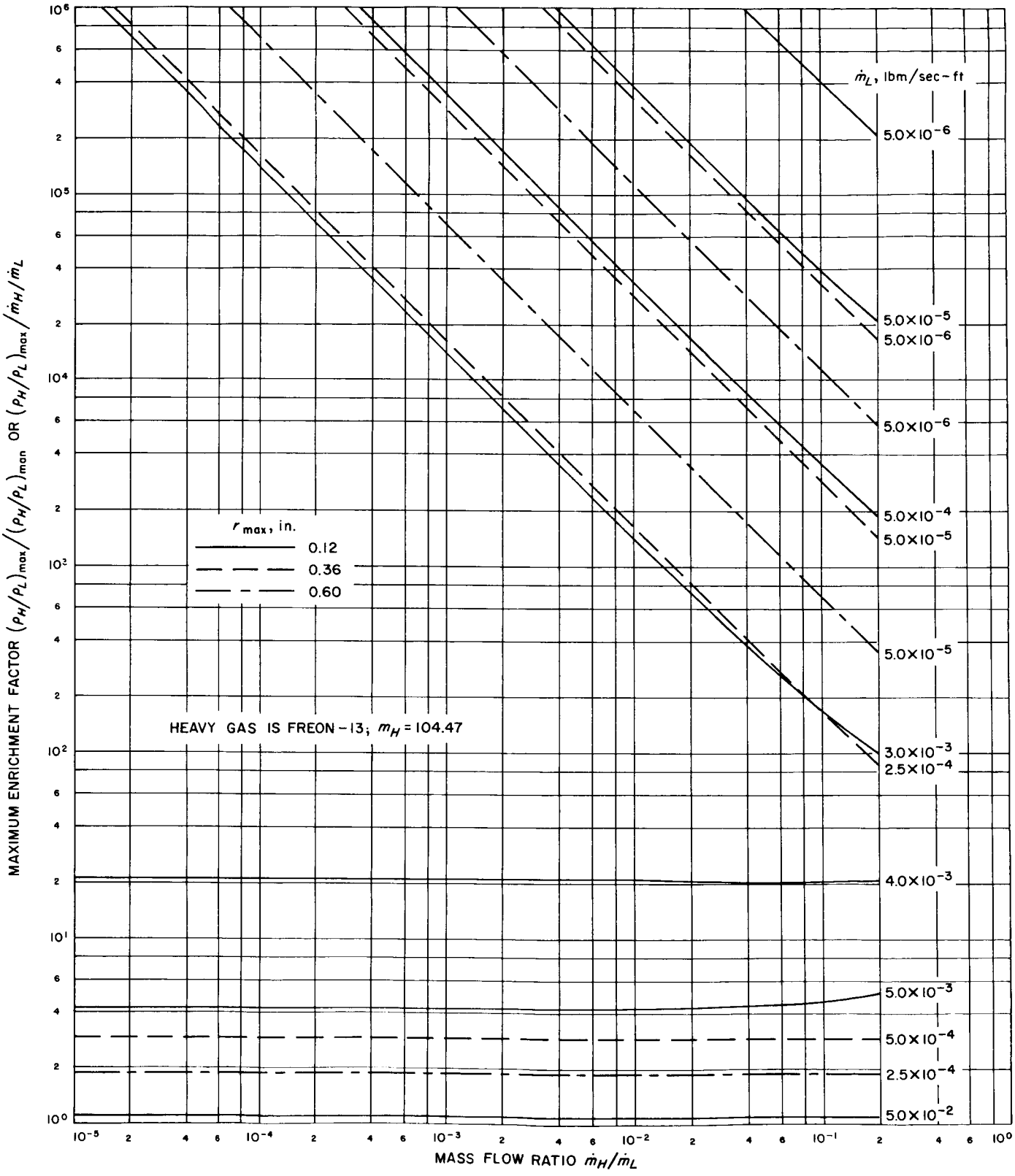

Fig. 5. Maximum enrichment factor for hydrogen–Freon-13 mixture

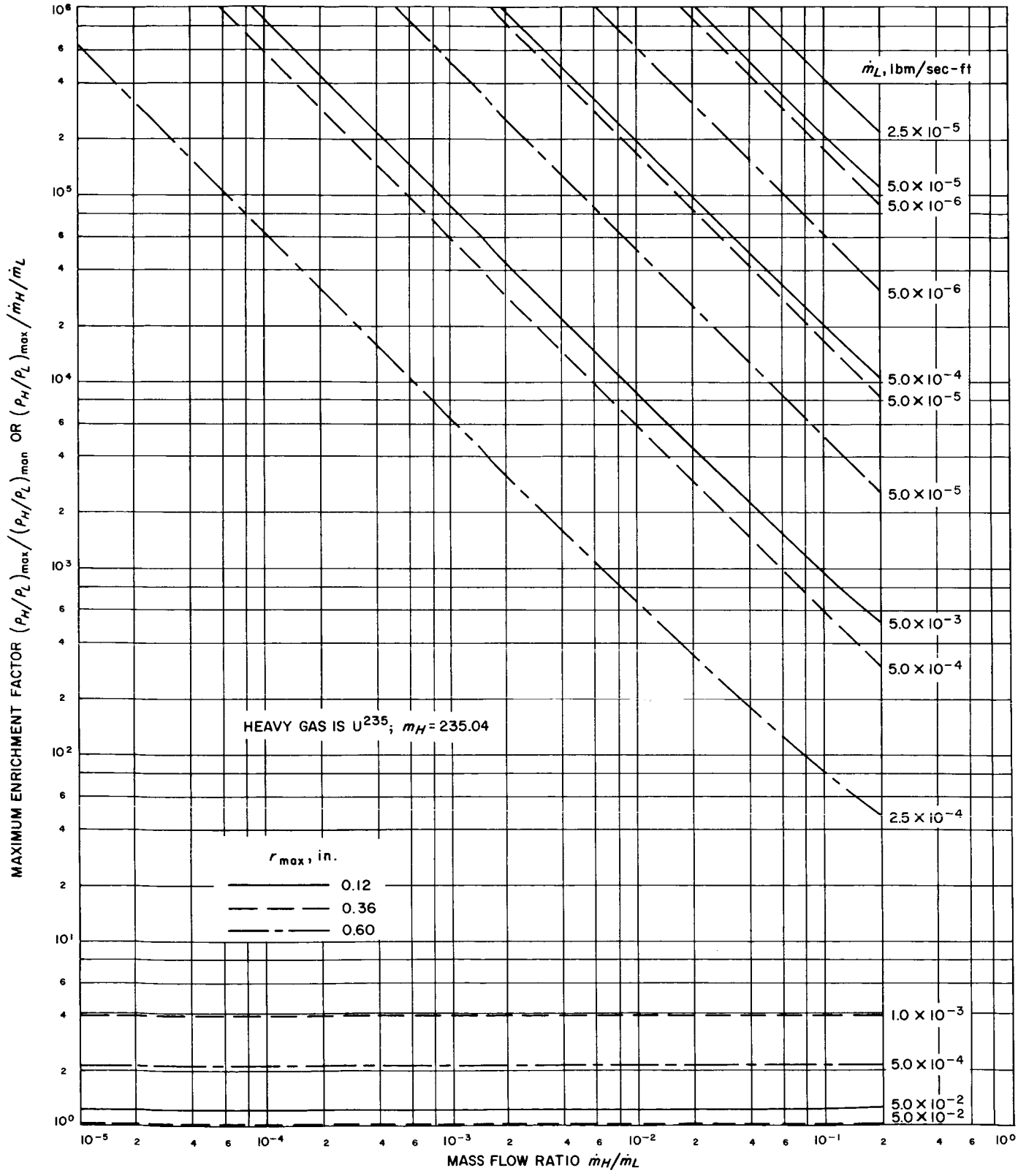

Fig. 6. Maximum enrichment factor for hydrogen–U^{235} mixture

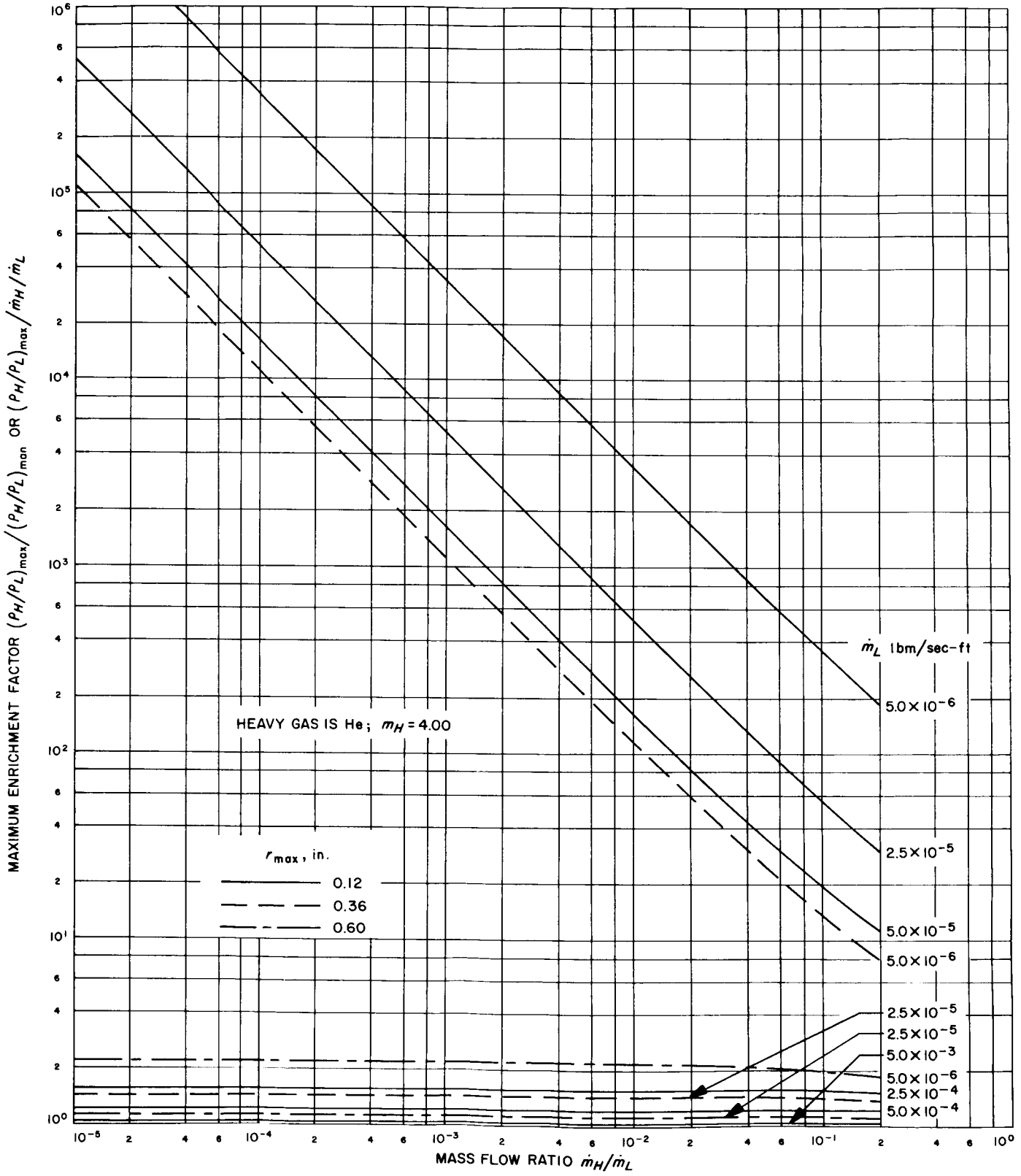

Fig. 7. Maximum enrichment factor for hydrogen–helium mixture

Hence, in order to satisfy criticality for the two propellant mass flow rates just mentioned, the wall pressure would have to be approximately 1.46×10^7 psia for $\dot{m}_L = 2 \times 10^{-3}$ lbm/sec-ft, and 1.06×10^2 psia for $\dot{m}_L = 10^{-3}$ lbm/sec-ft. This calculation clearly shows the desirability of operating the vortex tubes at a propellant mass flow rate that is less than critical, since by doing so the system pressure level can be kept to reasonable values.

Comparing Figs. 5, 6, and 7 with one another at any given value of $\dot{m}_H/\dot{m}_L$, $\dot{m}_L$, and r_{max}, the following expected result can be seen: as the heavy gas molecular weight increases, the maximum enrichment factor also increases. For the propulsion device this means that it would be desirable to use a fuel with as high a molecular weight as is obtainable since, as m_H increases, the propellant mass flow rate can also be increased while maintaining the desired maximum enrichment factor. For example, by increasing m_H by approximately a factor of two, the propellant mass flow rate can be increased five-fold, as can be seen by comparing Figs. 5 and 6.

4. Critical Mass Flow Rate $\dot{m}_{L_{crit}}$

To investigate the peculiar behavior of the maximum enrichment factor as the light gas mass flow rate is decreased, Eq. (5) was evaluated by varying $\dot{m}_L$ while all other parameters were held constant. A result of this computation is shown in Fig. 8 for one particular r_{max}, $\dot{m}_H/\dot{m}_L$, and binary gas mixture. All other parametric values are given in Table 1. The sudden increase in the maximum enrichment factor as the light gas mass flow rate decreases below a certain value is clearly illustrated.

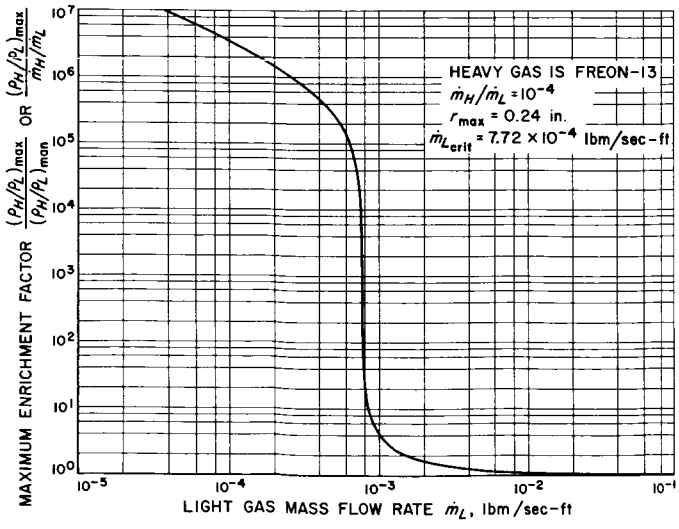

Fig. 8. Effect of mass flow rate on the maximum enrichment factor

The immediate cause of the sudden jump in the maximum enrichment factor is that the parameter b_0 in Eq. (5) passes through zero and becomes positive as $\dot{m}_L$ is reduced. The physical process that accounts for this sudden behavior is not understood. By this analysis however it is suggested that, for any given set of conditions, there exists a maximum flow rate $\dot{m}_L$ below which the vortex must operate if very large maximum enrichment factors are to be achieved. Of course, in practice several of the parameters, Γ in particular, depend on $\dot{m}_L$ and it remains to be seen whether an interesting flow and diffusion process can be generated at $\dot{m}_L$ below the critical value. The limitations of the apparatus used in the present investigation were such that $\dot{m}_L$ could not be decreased without decreasing Γ as well; hence an experimental verification of the existence of a critical mass flow rate could not be accomplished.

The light gas mass flow rate at the inflection point of Fig. 8 was chosen arbitrarily to characterize the rather sudden jump in maximum enrichment factor and will be called the critical mass flow rate $\dot{m}_{L_{crit}}$. To determine the dependence of $\dot{m}_{L_{crit}}$ on the other parameters, Eq. (5) was differentiated twice with respect to the light gas mass flow rate. The second derivative term in the resulting equation was set equal to zero and the equation solved for $\dot{m}_L$. Three roots were obtained, one real and two imaginary, with the one significant root given by:

$$\dot{m}_{L_{crit}} = C_0 \frac{b_1^{6/3} + b_1^{5/3} - b_1^{4/3} - b_1^{3/3}}{(b_1 + 1)^2} \tag{6}$$

where

$$C_0 = \frac{3 m_L^2 \left(1 - \frac{m_H}{m_L}\right)\left[\frac{1}{m_H}\left(1 + \frac{m_H}{m_L}\right)\frac{2\pi}{k g_c}\right]^{1/2} \Gamma^2}{8(\sigma_{LH})^2 r_{max}\left[T_\infty r_{max}^2 - \frac{(\dot{m}_H/\dot{m}_L + 1)\Gamma^2}{2 g_c C_{p_L}\left(1 + \frac{\dot{m}_H C_{p_H}}{\dot{m}_L C_{p_L}}\right)}\right]^{1/2}}$$

In Fig. 9, the critical light gas mass flow rate has been plotted as a function of b_1 with C_0 as a parameter (b_1 is the ratio of light to heavy gas particle flow rate $\dot{n}_L/\dot{n}_H$). It can be seen that the critical mass flow rate is very nearly independent of the variable b_1 and approximately equal to the parameter C_0. Therefore, one can increase the propellant flow rate and still maintain a high enrichment factor if the circulation $2\pi\Gamma$ and/or the heavy gas molecular weight m_H is increased. Conversely, a lack of circulation can be compensated for by choosing a heavy gas

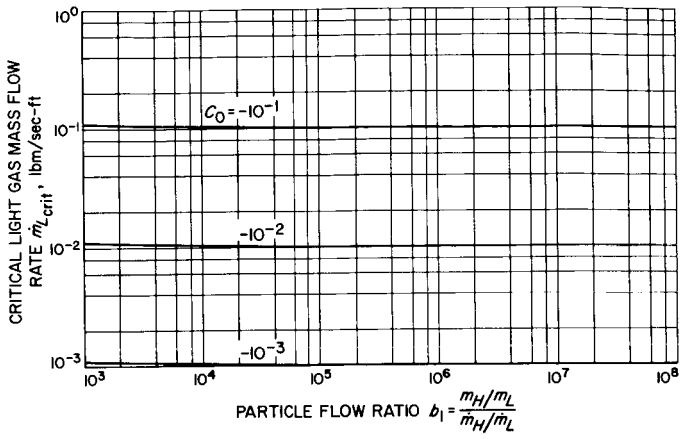

Fig. 9. Effect of the groups b_1 and C_0 on the critical mass flow rate

of greater molecular weight. These results are also subject to the behavior of r_{max} with Γ and m_H.

B. End-Wall Static Pressure Measurements

The radial static pressure distribution was measured on the surface of the closed end wall for several values of mass flow rate, exit-hole diameter, and sampling probe diameter and location.

1. Effect of Exit-Hole Diameter and Mass Flow Rate on the End-Wall Static-Pressure Distribution

The results of typical radial static-pressure distributions as measured on the closed end wall of vortex tube A, using hydrogen and nitrogen gases independently, are shown normalized with respect to the cylindrical wall static pressure in Fig. 10. It is seen that the two pressure distributions are very similar and that the hydrogen static pressure is slightly greater than the nitrogen pressure for all radii less than the cylindrical wall radius. This type of comparative experiment was repeated for cylindrical wall static pressures of 100, 150, 370, and 500 cm Hg (abs). It was found that the pressure distributions were qualitatively the same for all but the lowest pressure level, and that for all cases the hydrogen pressure was greater than that of the nitrogen. At a cylindrical wall static pressure of 100 cm Hg (abs), the differences between the hydrogen and nitrogen pressures were more pronounced and varied from zero at the cylindrical wall radius to 7.2 cm Hg at the centerline where the nitrogen pressure was found to be 41.4 cm Hg (abs). From these results, it appears that the large number of radial pressure distributions obtained with nitrogen, and analyzed in Ref. 8,

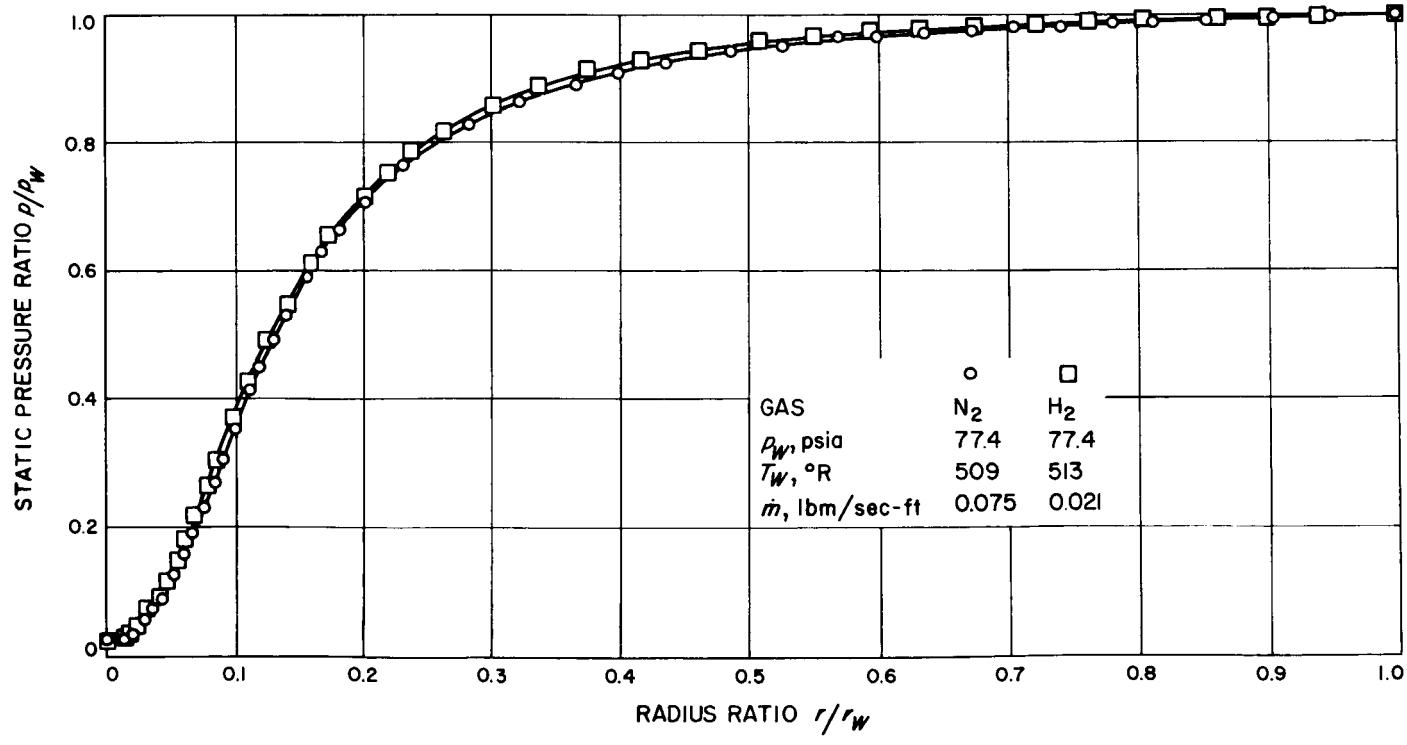

Fig. 10. A comparison of the radial static pressure distributions for hydrogen and nitrogen gases

can be applied to the hydrogen vortex, providing the cylindrical wall static pressure is high enough.

Of the four possible driving potentials in the equation for binary diffusion described in Ref. 9, the one dominating potential that is controllable in the vortex-type gaseous core nuclear reactor concept of Ref. 1 is the radial pressure gradient $d \ln p/dr$. The coefficient of this pressure gradient term in the diffusion equation is a function of the molecular masses, partial mass densities, and mixture temperature only. It is of interest, therefore, to determine the magnitude and radial distribution of the radial pressure gradient in these vortex-type flows. For a binary mixture of perfect gases, the static pressure is given by $p = n_L (1 + n_H/n_L)\, kT$ where n_L and n_H are the particle densities of the low and high molecular weight species, respectively, k is Boltzmann's constant, and T is the equilibrium temperature of the mixture. In the binary system of interest for the vortex-type gaseous core nuclear reactor concept, $n_H << n_L$; therefore the static pressure is mainly determined by the propellant or low molecular weight species and can be expressed as $p = n_L kT$. Because of this approximation, the measurements of the radial pressure distributions were made in a single-component vortex. Also, since the difference between the radial pressure distributions obtained with hydrogen and nitrogen is small for the flow conditions of interest, nitrogen was used to determine the radial pressure gradient and its radial distribution. It is assumed here that this difference remains small for all exit-hole diameters.

The radial static-pressure distribution on the closed end wall of vortex tube A was measured for several exit-hole diameters and for several values of the cylindrical wall static pressure at each exit hole. For these measurements, the fluid was exhausted into the atmosphere through a cylindrical hole 0.99 in. long and of various diameters at the center of one end wall (Fig. 2). Neither center plug nor sampling probe was used in these experiments.

The radial distribution of the radial pressure gradient

$$\frac{d \ln p/p_W}{d\, r/r_W}$$

were computed for several representative conditions by graphically differentiating the pressure distributions normalized with respect to the cylindrical wall static pressure and then dividing by the pressure ratio. These representative distributions are shown in Figs. 11 and 12.

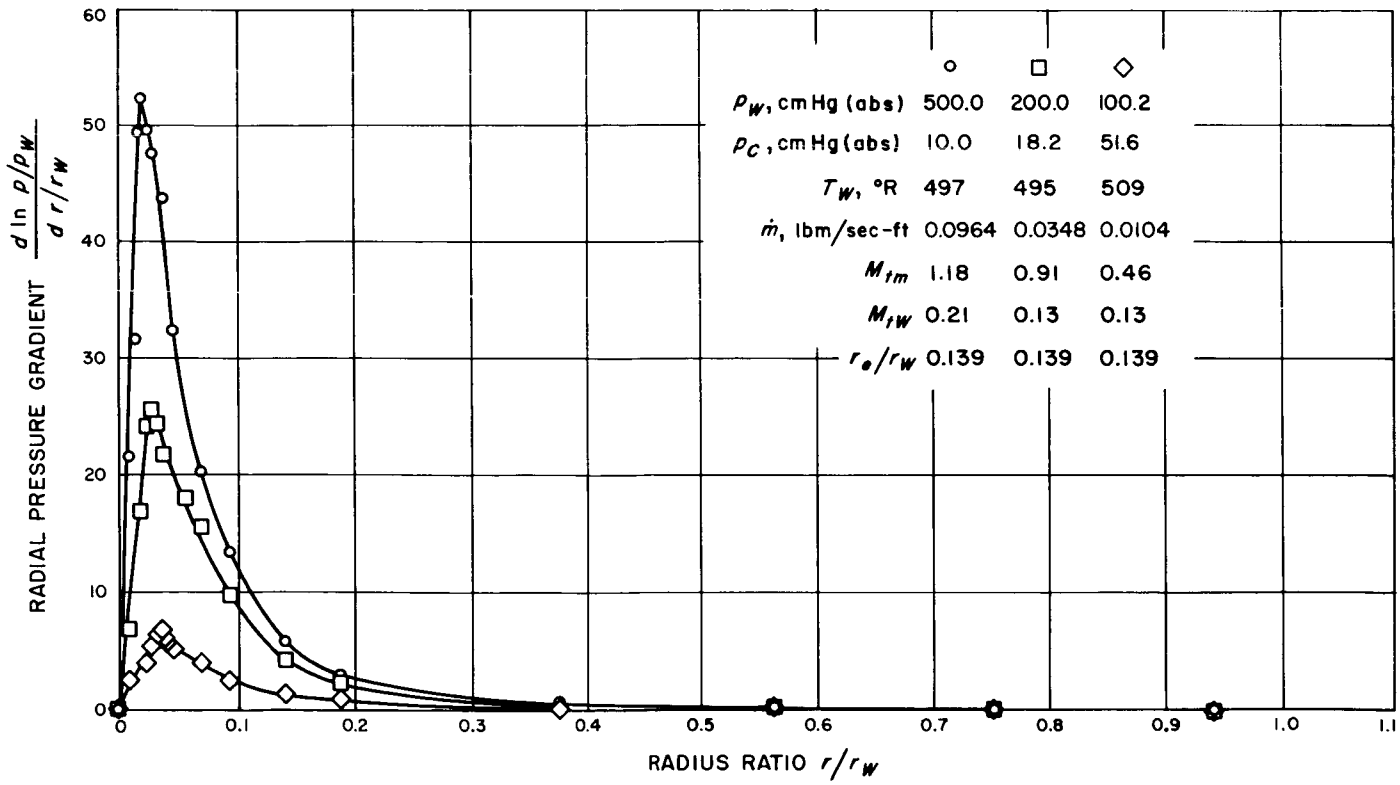

Fig. 11. Effect of mass flow rate on the radial distribution of the radial pressure gradient

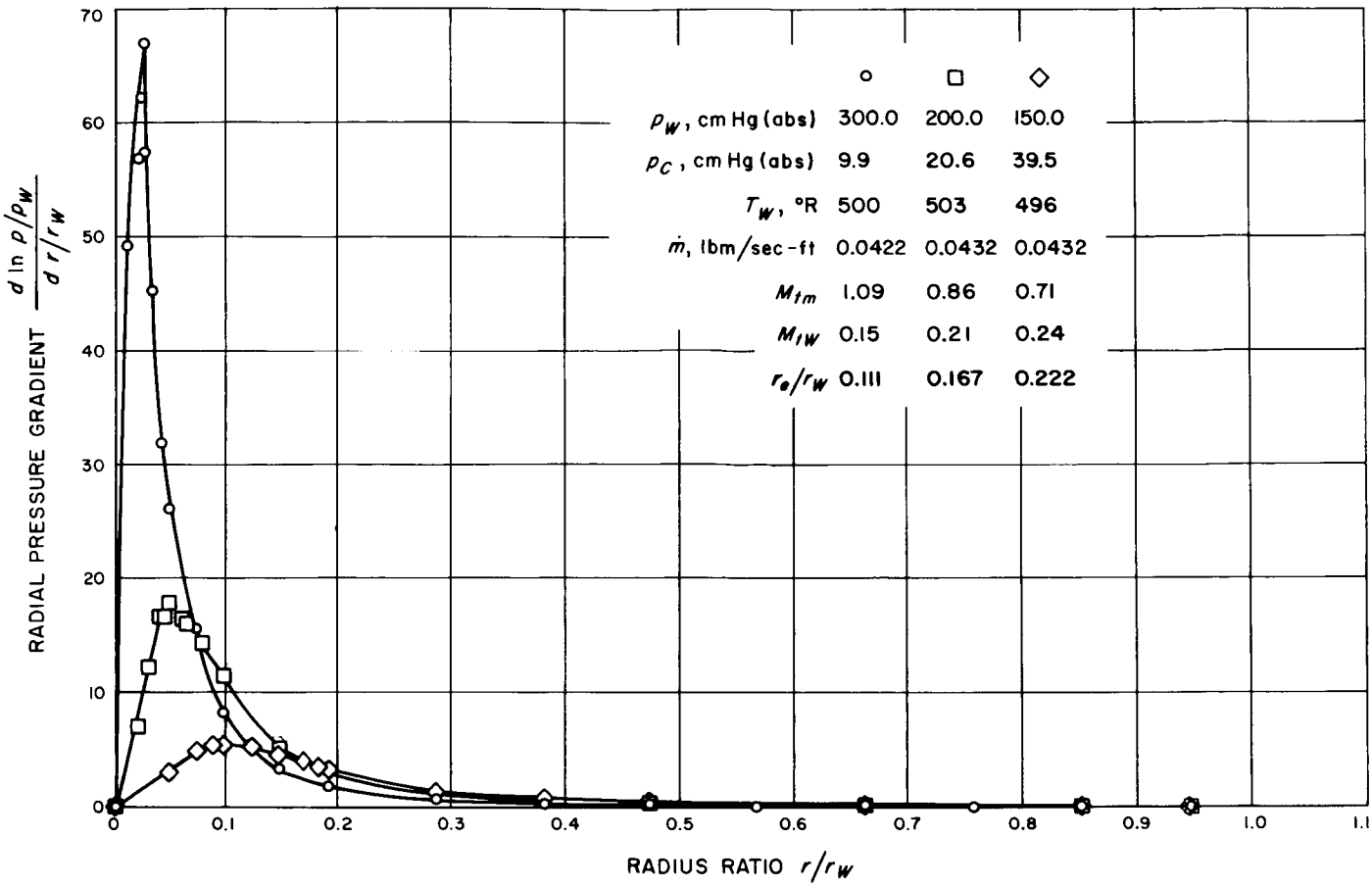

Fig. 12. Effect of exit-hole radius on the radial distribution of the radial pressure gradient

To obtain the results in Fig. 11, the ratio of exit-hole to vortex tube diameter was fixed at 0.139, and the radial pressure distribution was measured for cylindrical wall static pressures of 100.2, 200.0, and 500.0 cm Hg (abs). The magnitude of the radial pressure gradient is finite but very small at the cylindrical wall and rises monotonically to a maximum near the vortex centerline, then drops to zero at the centerline. As the cylindrical wall static pressure is increased, the maximum value of the radial pressure gradient increases and its radial position is displaced slightly inward. These results are not general and their limitations will be discussed subsequently. Note in Fig. 11 that as the total mass flow rate into the vortex tube increases, the cylindrical wall static pressure also increases since the exit-hole diameter is held constant. A variation in either of these quantities can have a significant effect on the flow, as shown in Ref. 8. The effects of varying the exit orifice radius while holding the mass flow rate approximately constant are shown in Fig. 12. In order to hold the mass flow rate constant, the cylindrical wall static pressure had to increase as the exit-hole diameter decreased. Again the radial pressure gradient was found to be finite but very small at the cylindrical wall and to increase to a maximum, then drop to zero at the centerline. Decreasing the exit-hole diameter by a factor of two caused the maximum pressure gradient to increase by better than one order of magnitude, and its radial location to shift inward by a sizable amount. Note also that as the exit-hole diameter is decreased, the fluid tangential acceleration or increase in radial pressure gradient is delayed until the fluid reaches smaller radii.

The maximum value of the radial pressure gradient has been determined from each of several additional experiments; all are plotted vs mass flow rate per foot of vortex tube length, with exit-hole diameter and cylindrical wall static pressure as parameters, in Fig. 13. As can be seen, the rate of change of the maximum pressure gradient with mass flow rate is a strong function of exit-hole diameter and cylindrical wall static pressure for the low flow rates and smaller exit holes. Also, it appears that the maximum pressure gradient approaches a maximum for each exit-hole diameter and approaches a minimum for each cylindrical wall pressure. The radial positions of the

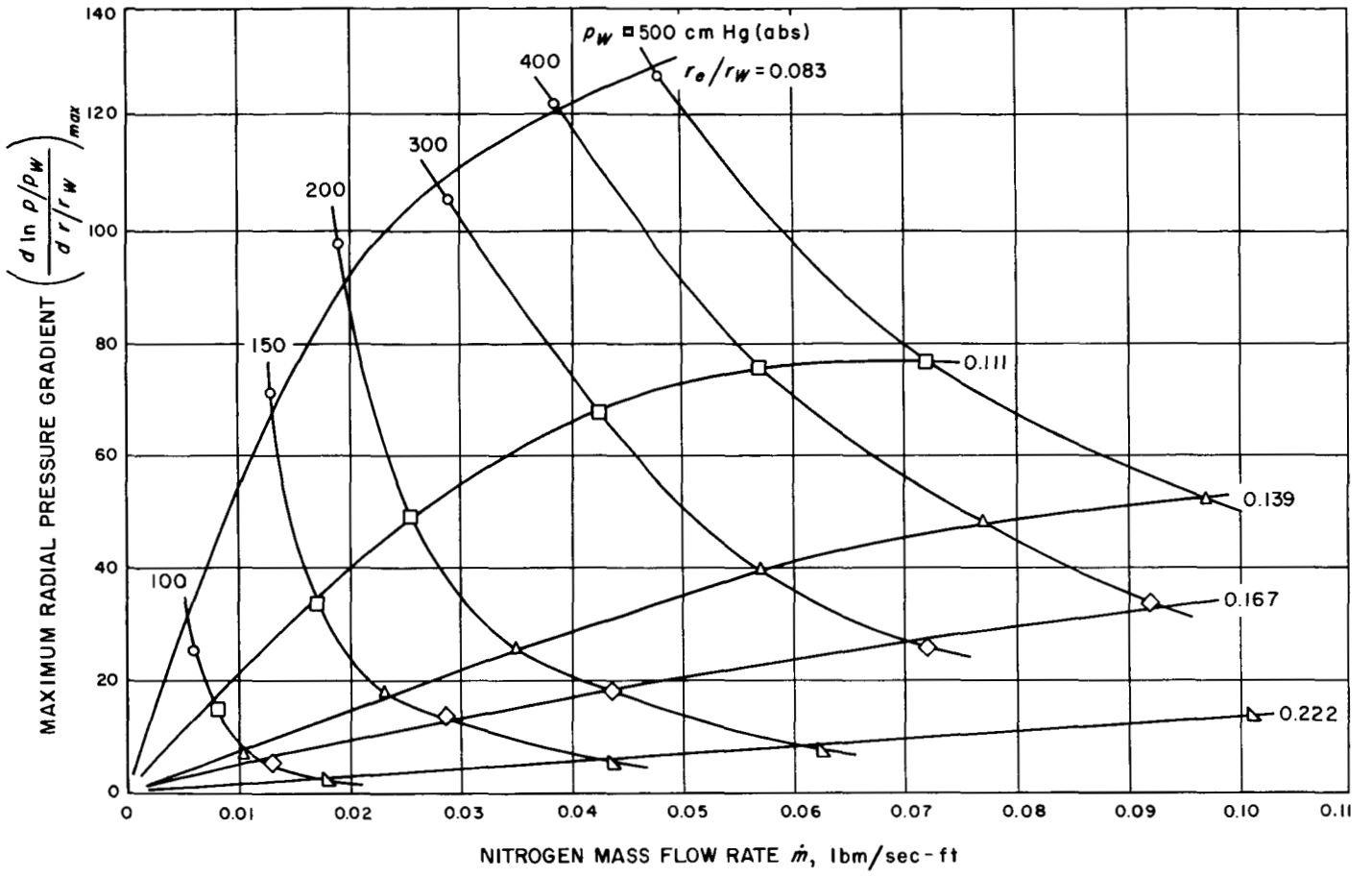

Fig. 13. Effects of exit-hole radius, pressure level, and mass flow rate on the maximum radial pressure gradient

maximum radial pressure gradient corresponding to the points of Fig. 13, are shown in Fig. 14. It can be seen that for any given exit-hole diameter the shift inward is slight as the mass flow rate increases, but that the shift is relatively great as the exit-hole diameter is decreased at either constant mass flow rate or constant cylindrical wall static pressure at the low pressure levels. Note also that under all conditions investigated, the maximum radial pressure gradient occurs well inside the exit-hole radius.

2. Effect of Sampling Probes on the End-Wall Static-Pressure Distribution

Since very little quantitative information on probe effects in rotating flows is available, a limited experimental investigation was made in order to determine the magnitude and nature of these disturbances. The experiments were performed in vortex tube B, with nitrogen. Only probes that were similar to the sampling probe described in this Report were investigated. Variations in exit-hole diameter, probe axial location, and mass flow rate were made, and measurements were taken to indicate the effect of probe diameter at each condition.

The detailed effect of this type of probe on the radial static pressure distribution, as measured on the closed end wall, is shown in Fig. 15. The probe diameter was 0.042 in. and the probe was located 8.00 in., or 2.67 vortex tube diameters, from this end wall. Introduction of the probe caused the cylindrical wall static pressure to drop from 205 to 182 cm Hg (abs) while the manifold pressure was held constant at 280 cm Hg (abs). The wake of the probe must act as a shunt, much the same as the end-wall boundary layers discussed in Ref. 2, providing a secondary path through the vortex for part of the injected fluid. This secondary path, both in the probe wake and end-wall boundary layers, must offer less resistance to the radial flow, resulting in the observed decrease of cylindrical wall static pressure as the probe is inserted. The result of the decreased cylindrical wall static pressure was to increase the tangential velocity near the cylindrical wall (Ref. 8), and this was reflected as an increased

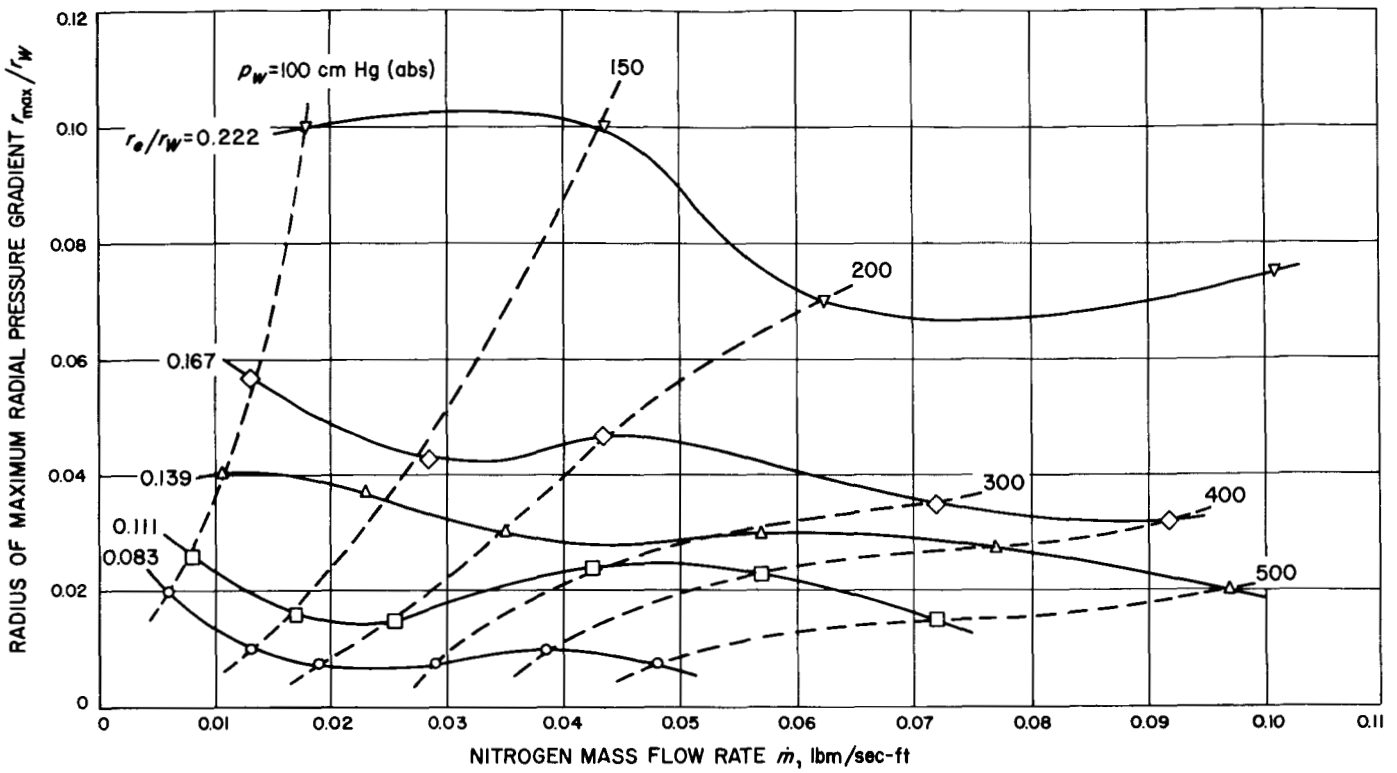

Fig. 14. Radial location of the maximum radial pressure gradient

radial pressure gradient at large radii. However, this increase in tangential velocity was restricted to regions near the cylindrical wall; actually, the probe decreases the tangential velocity in the rest of the flow field. To keep the cylindrical wall static pressure the same, with and without the probe in position, as is shown in Fig. 15, the manifold pressure had to be increased by 12% when the probe was introduced. This increase in manifold pressure and hence in mass flow rate, necessitated by the introduction of the probe, also produced a decrease in static-pressure ratio varying from zero at the cylindrical wall to 0.6% at the centerline. In Fig. 15, note the increased radial pressure gradient at large radii, in this case caused by the increased mass flow rate since the cylindrical wall static pressure was held constant. Note also the decrease in the maximum radial pressure gradient, and hence tangential Mach number, caused by the probe and its wake shunting fluid from the vortex free stream. Since the binary diffusion process in a vortex flow is strongly dependent on the radial pressure gradient, this type of probe disturbance is extremely important.

To investigate the gross effect of probe diameter on vortex strength at various mass flow rates, the pressure difference between the cylindrical wall and the centerline was measured on the closed end wall. This pressure difference Δp, normalized with respect to itself with no probe inserted, is shown in Fig. 16. Probe diameters varying from 0.003 to 0.042 in. were inserted at a station 8.00 in. from the closed end wall, and the mass flow rate was varied from 0.025 to 0.052 lbm/sec by varying the manifold pressure. It is again apparent that changes in mass flow rate have little effect on the gross nature of the disturbance. However, the strong effect of probe size on the gross vortex performance indicates the need for keeping the probe diameter at a minimum.

For three different exit-hole diameters but constant manifold pressure and with no probes inserted, the radial distributions of the tangential Mach number M_t were computed from the radial static-pressure distributions as measured on the closed end wall, from the following form of the radial momentum equation:

$$M_t = \left(\frac{r/r_w}{\gamma} \times \frac{d \ln p/p_w}{d\, r/r_w} \right)^{1/2} \qquad (7)$$

where γ is the ratio of specific heats. An experiment was then performed at the same manifold pressure in order to determine the tangential Mach number at the radius at

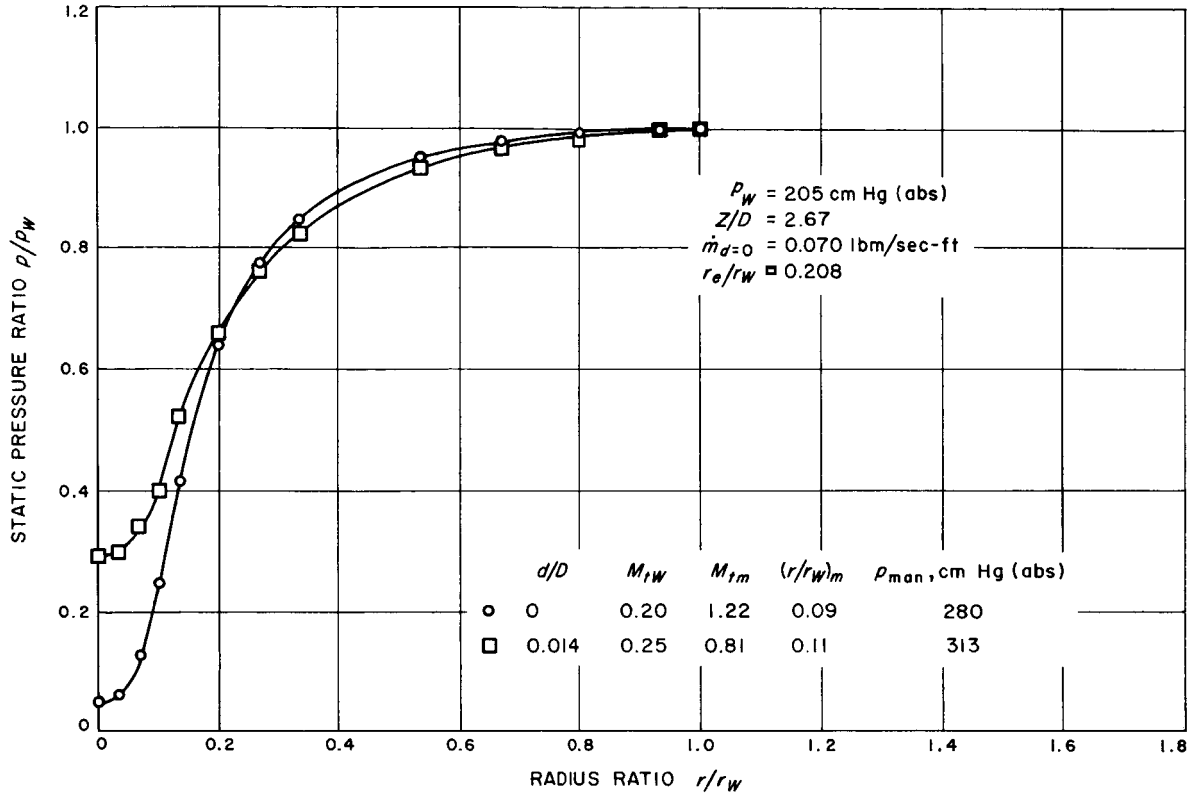

Fig. 15. Effect of sampling probe on the radial static pressure distribution

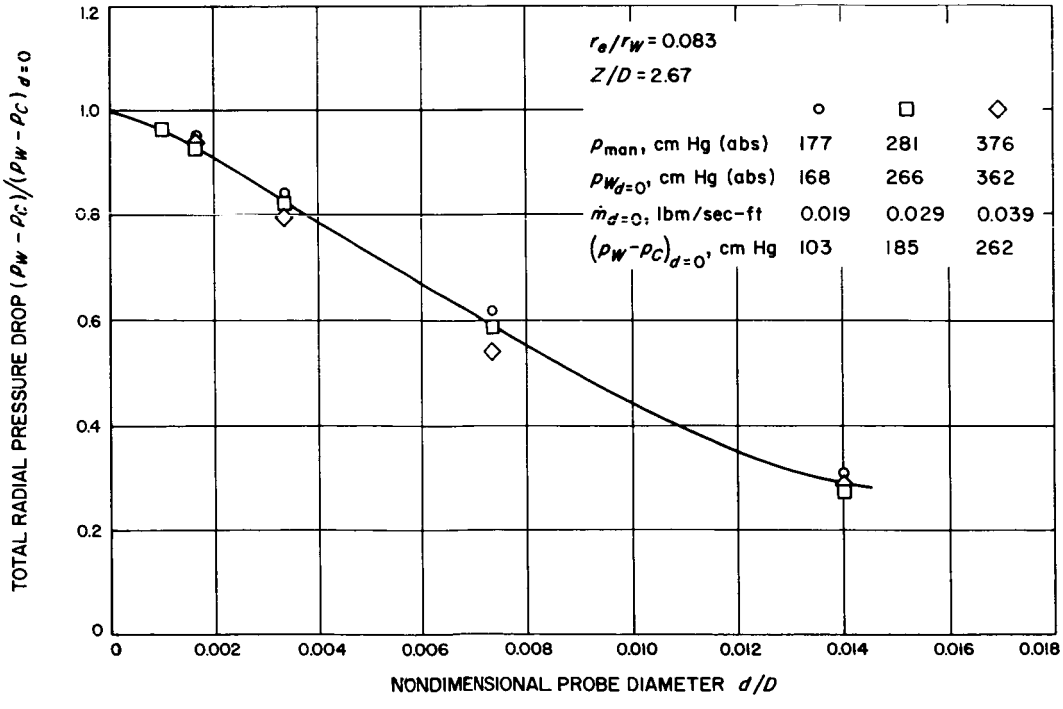

Fig. 16. Effect of sampling probe diameter on the pressure drop across the vortex

which the tangential Mach number for the no-probe experiment was found to be a maximum for each of several probe diameters, and for each of several exit-hole diameters. The ratio of this approximate maximum tangential Mach number M_{tm} to the undisturbed maximum $(M_{tm})_{d=0}$, is shown in Fig. 17 as a function of probe diameter with exit-hole diameter as a parameter. It can be seen that for any given probe diameter, the decay of the tangential Mach number is reduced by increasing the exit-hole diameter. This result is probably due to an increase in the tangential Mach number near the cylindrical wall, the maximum tangential Mach number, and the mass flow rate, or to what is tantamount to a general increase in the total vortex strength as the exit-hole diameter is increased while the manifold pressure is held constant. It is again apparent that the probe diameter must be kept small in order to minimize this disturbing influence.

To investigate the axial distribution of the disturbance caused by the sampling probe, a 0.042-in.-D probe was moved axially toward the closed end wall, in discrete steps. Again, the pressure gradient at the radius of the undisturbed maximum tangential Mach number was determined and converted into tangential Mach number; results are shown in Fig. 18. It appears that the entire vortex flow is disturbed equally by the presence of a probe. This is not surprising since large axial pressure gradients would be difficult to support in this type of flow. Of course, the probe's wake, like the end-wall boundary layers, generates secondary flows that alter the velocity field in the axial direction, but this effect is not discernible from end-wall pressure measurements. As expected, when the probe was placed in the end-wall boundary layer the pressure distribution on that end wall was completely changed and could not reflect the effect of the probe on the primary vortex flow.

C. *Measurements of the Heavy to Light Gas Mass Density Ratio*

The local effect of the radial pressure gradient on a binary mixture was determined for three values of the cylindrical wall static pressure and for an exit-hole diameter of 0.625 in.

1. Low-Strength Vortex ($\dot{m}_{H_2} = 0.0042$ lbm/sec-ft)

a. Pressure and Mach number distributions. The radial distributions of static pressure and tangential Mach number corresponding to the minimum cylindrical wall static

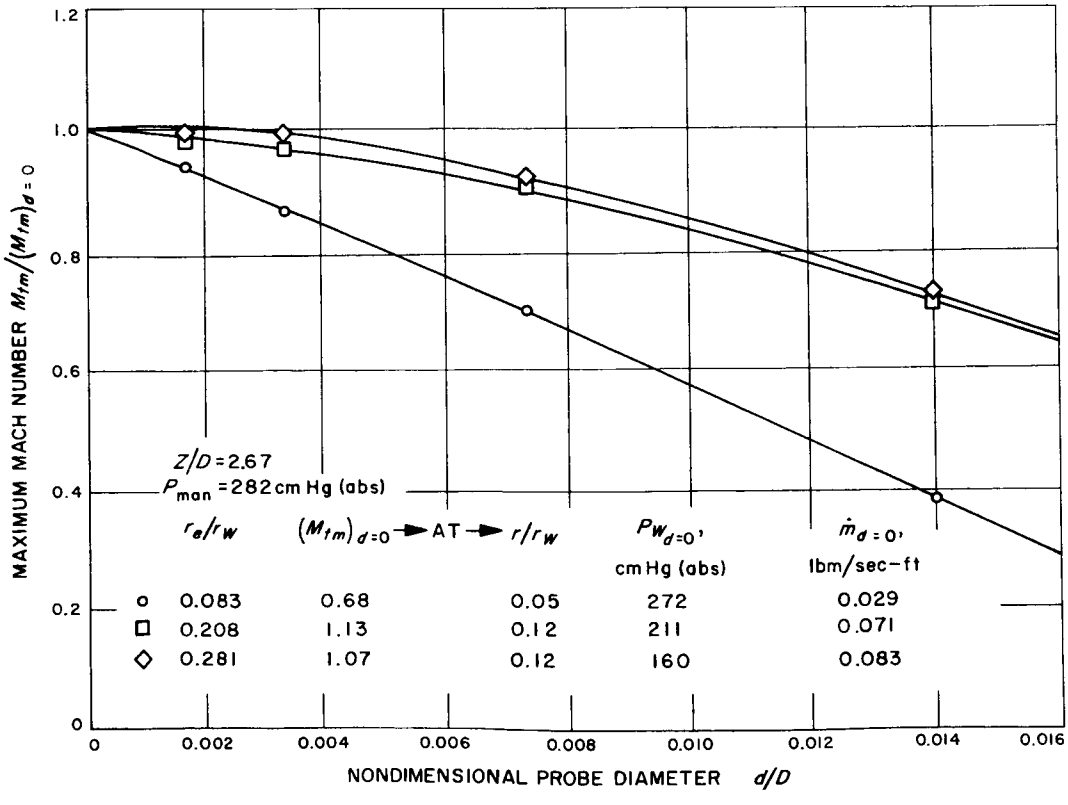

Fig. 17. Effect of sampling probe diameter on the maximum Mach number

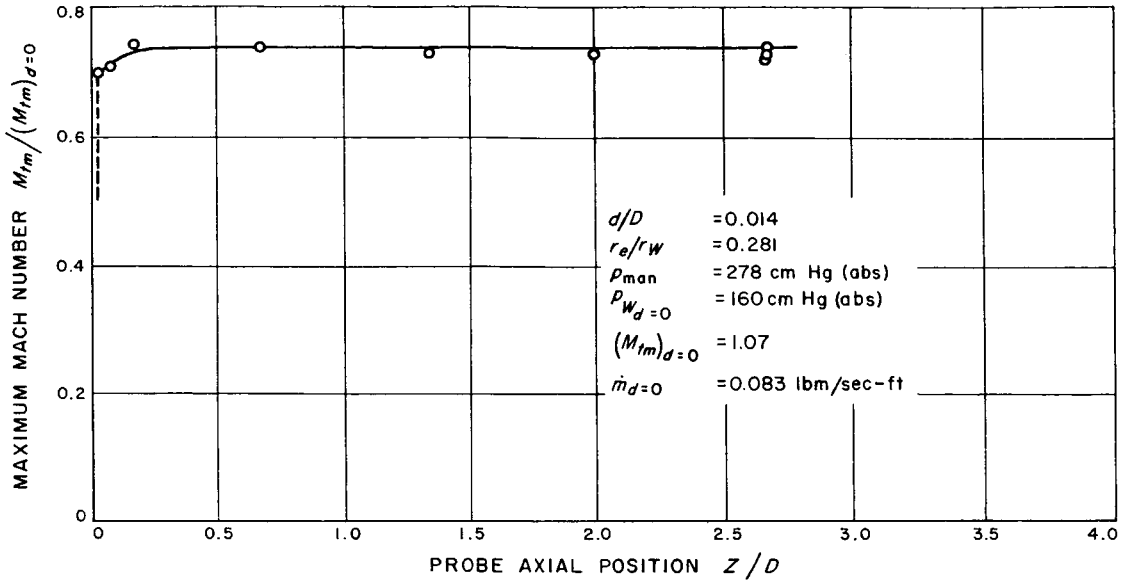

Fig. 18. Effect of sampling probe axial position on the maximum Mach number

pressure used are shown in Fig. 19. This pressure distribution, measured in a pure hydrogen vortex on the closed end wall of the vortex tube, was obtained with the 0.010-in.-D sampling probe installed at a station midway between the end walls ($Z/D=2.68$). The exit-hole center plug was adjusted axially until the centerline pressure at the closed end wall was minimized. At this position, the exit gap δ was 0.040 in. and the corresponding exit area was 0.18 in^2. Note that the tangential Mach number distribution displays a minimum at a radius ratio of approximately 0.8. This behavior seems to be characteristic of the Mach number distribution obtained at low mass flow

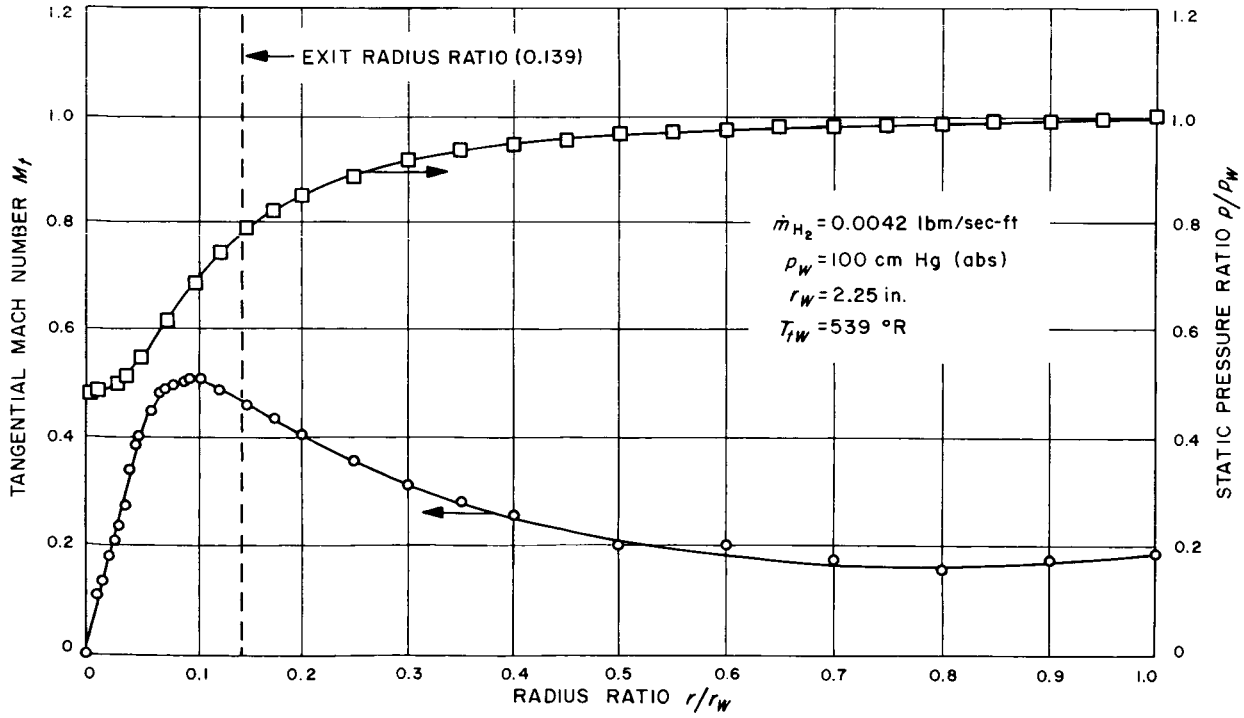

Fig. 19. Radial static pressure and tangential Mach number distributions for low-strength vortex

rates and can be predicted (Ref. 10) by taking into account, in a simple way, the effect of friction on the cylindrical and end walls of the vortex tube.

b. Effect of heavy gas mass flow rate. Argon was injected at a measured rate into the hydrogen and the two gases were premixed before they were injected into the vortex tube. The radial distribution of the ratio of argon to hydrogen mass densities ρ_H/ρ_L was measured at the midstation ($Z/D=2.68$) and is shown normalized with respect to the density ratio in the vortex tube manifold $(\rho_H/\rho_L)_{man}$, in Fig. 20. The ratio of argon to hydrogen mass flow rates was 0.0240 and is equal to the mass density ratio of the mixture in the vortex tube manifold. Distributions, such as those in Fig. 20, show directly the effect of the pressure-gradient-induced diffusion on the homogeneous binary gaseous mixture, since, if there were no diffusion, the density ratio would be constant for all radii and equal to the density ratio in the vortex tube manifold. This profile displays characteristic gradual increase of density ratio with decreasing radius at large radii, a maximum ratio at a relatively small radius, and then a sharp decrease to the minimum density ratio near the vortex tube centerline. However, only the profiles obtained at this low hydrogen mass flow rate have that peculiar inflection point evident at a radius ratio of 0.13 (Fig. 20), and a rather broad distribution near the maximum density ratio. A second profile was obtained under the same conditions, except that the argon mass flow rate was reduced by approximately a factor of two. For comparison, this second profile is also shown in Fig. 20. Note that the density ratio relative to that in the manifold (enrichment factor) increases as the heavy gas mass flow rate decreases. This effect seems to be exaggerated in the figure, possibly because of some uncorrectable drift in the original data; however, it will be shown below that this effect is generally true. Both profiles reach their minimum at a finite radius, then increase as r is reduced further. This behavior is also general and will be discussed further in a subsequent section.

By using the experimentally determined boundary conditions and parametric values listed in Fig. 20, analytic density ratio distributions were computed from Eq. (2) and are shown for comparison in Fig. 20. For this computation, and for all others to follow, it was assumed that

$$T_\infty = T_{t_W}$$

$$\dot{m}_H/\dot{m}_L = (\rho_H/\rho_L)_{man}$$

$$\Gamma = M_{t_{(at\ \bar{r}_{max})}} \times \bar{r}_{max} \times (\gamma_L g_c R_L T_{t_W})^{1/2}$$

and the binary collision cross section σ_{LH} was estimated by the methods of Ref. 11. Also, $\bar{r}_{max}$ was taken as the average radial location of the maximum density ratio for each hydrogen mass flow rate used. In addition, Eq. (3) was inverted to obtain

$$\dot{m}_L = -\frac{(\rho_H/\rho_L)_{max}}{\dot{m}_H/\dot{m}_L}\frac{\Gamma^2}{r_{max}} \times \frac{(T_\infty r_{max}^2 - a_1)^{-1/2} m_L^2\left(1-\frac{m_H}{m_L}\right)}{\left[\frac{1}{a_5}(\rho_H/\rho_L)_{max}^2 + \frac{a_4}{a_5}(\rho_H/\rho_L)_{max} + 1\right]} \times \left[\frac{\left(1+\frac{m_H}{m_L}\right)}{m_H}\frac{2\pi}{kg_c}\right]^{1/2}\frac{3}{8(\sigma_{LH})^2} \tag{8}$$

This gives a means of determining the theoretical light gas mass flow rate $\dot{m}_L$, based on the experimentally determined parameters, that is necessary to place the maximum density ratio at the point at which it was found experimentally. The light gas mass flow rate, computed in this way for the two experiments shown in Fig. 20, indicates that $\dot{m}_L$ decreased by a factor of two as $\dot{m}_H/\dot{m}_L$ decreased by the same amount. It is unlikely that $\dot{m}_L$ actually decreased in the experiments since the only significant difference between the two experiments was a small change in the heavy gas mass flow rate and this variation could not effect such a change in the basic flow field. Therefore this apparent variation of $\dot{m}_L$ is caused by the difference between the theoretical model and the actual flow, or an error in the experimentally determined parameters. If it was caused by an error in the experiments, Eq. (8) serves to indicate the type of errors responsible. To illustrate, Eq. (8) can be approximated, for this problem, by the following:

$$\dot{m}_L \approx \frac{\text{constant}}{r_{max}^2\left[\frac{\dot{m}_H/\dot{m}_L}{(\rho_H/\rho_L)_{max}} - 1\right]} \tag{9}$$

Therefore, if in fact the maximum enrichment factor increases as the ratio of mass flow rates decreases, r_{max} should also decrease. Although the experimental distributions of Fig. 20 are too broad to determine a change in r_{max}, other experiments, to be discussed subsequently, do show a slight decrease in r_{max} as $\dot{m}_H/\dot{m}_L$ is reduced. Note that if r_{max} does decrease as $\dot{m}_H/\dot{m}_L$ decreases, the increase of the maximum enrichment factor is even greater than is shown by the curves of Figs. 5, 6, and 7. The ratio of the theoretical light gas mass flow rate to the hydrogen mass flow rate used in the experiment,

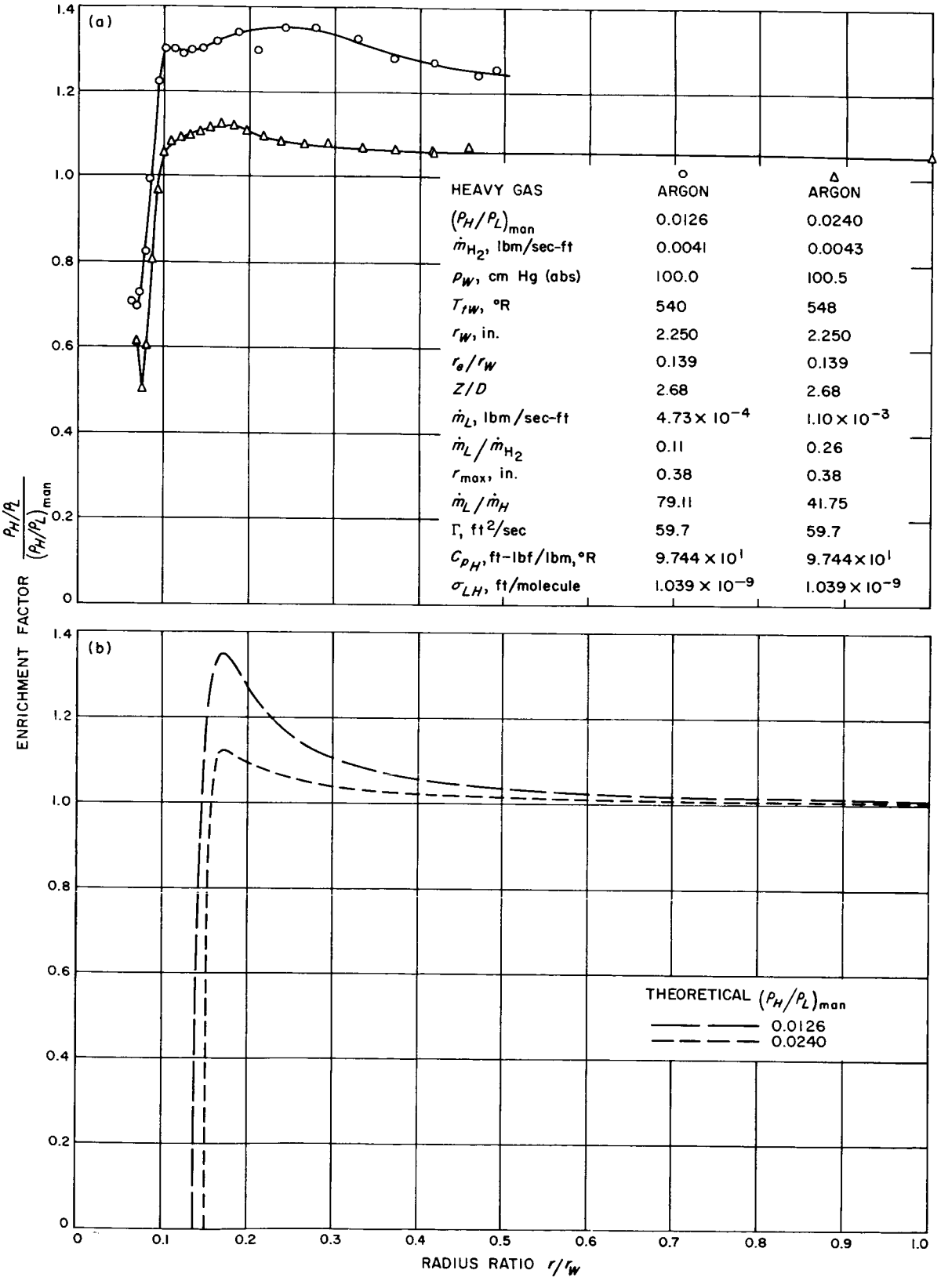

Fig. 20. Effect of heavy gas mass flow rate on the density ratio distributions

$\dot{m}_L/\dot{m}_{H_2}$, is also shown in Fig. 20. Additionally, this figure shows the experimental density ratio distributions to be broader than the corresponding analytic distributions. This result was found for all comparisons made and might be due to the influence of the sampling probe or turbulence.

c. Effect of heavy gas molecular weight. To investigate the effect of heavy gas molecular weight on the density ratio distributions, Freon-13 (chlorotrifluoromethane) with a molecular weight of 104.5 and Freon-13B1 (bromotrifluoromethane) with a molecular weight of 148.9 were substituted, in turn, for the argon in the experiment described above. The radial distributions of the mass density ratio for the three heavy gases at approximately the same heavy gas mass flow rate are shown in Fig. 21.

For each heavy gas, the distributions show the same general characteristics. The principal differences are that the maximum and minimum enrichment factors increase and decrease, respectively, with increasing molecular weight. It is believed that these differences would be more pronounced if, in each of the experiments of Fig. 21, the ratio of mass densities in the vortex tube manifold were the same. The measured density ratio at the vortex tube cylindrical wall is greater than the ratio in the vortex tube manifold, a result that was found in all the experiments performed.

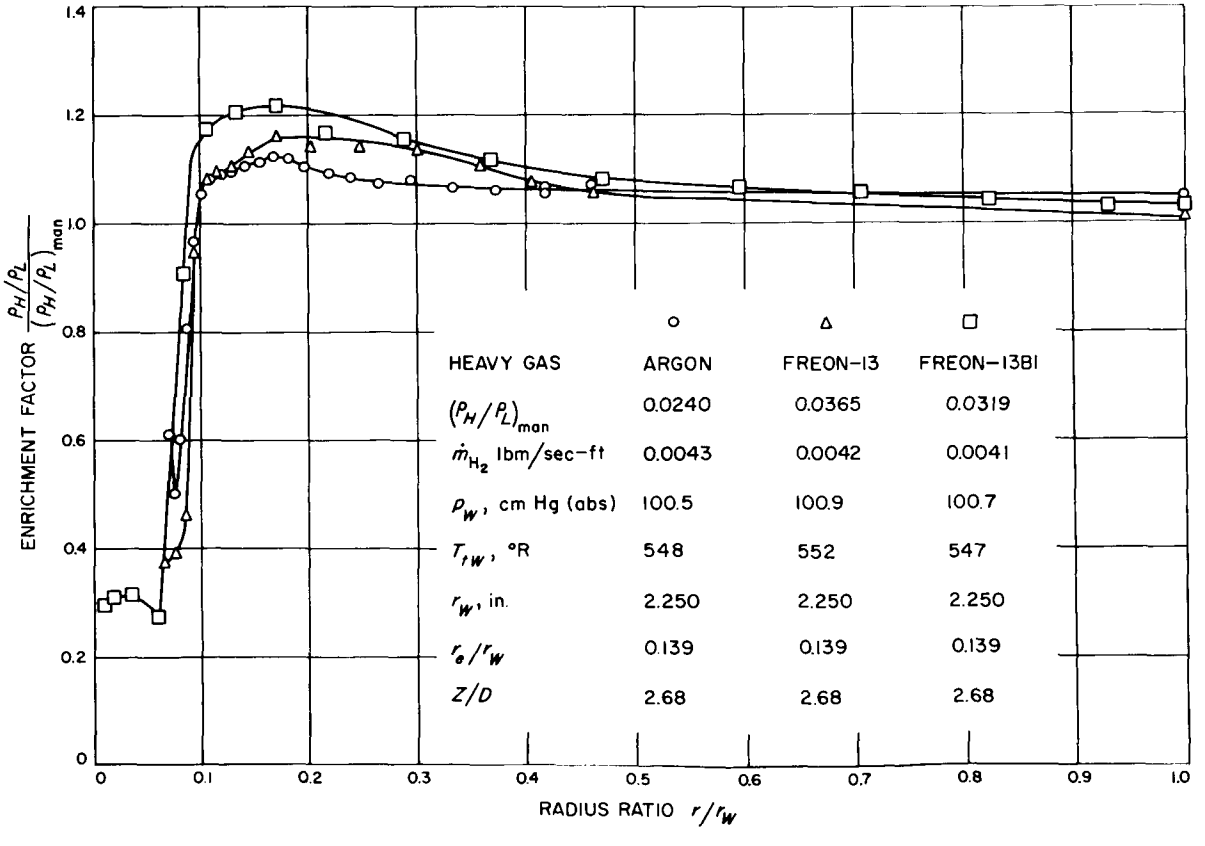

Fig. 21. Effect of heavy gas molecular weight on the density ratio distributions

2. Medium-Strength Vortex ($\dot{m}_{H_2} = 0.0085$ lbm/sec-ft)

a. Pressure and Mach number distribution. With a cylindrical wall static pressure of 150 cm Hg (abs) and the 0.010-in.-D sampling probe installed at the station nearest the closed end wall ($Z/D = 0.17$), the radial distribution of static pressure was measured for a pure hydrogen flow. For this hydrogen mass flow rate of 0.017 lbm/sec, the optimum position for the center plug was found when $\delta = 0.057$ in. and the exit area was 0.26 in^2. This distribution, together with the computed radial distribution of tangential Mach number, is shown in Fig. 22. The static pressure on the end wall containing the exit orifice was also measured and is shown for comparison in Fig. 22. Note that the cylindrical wall static pressure, measured on the two end walls, differs by approximately 1%. This was confirmed by using a water-filled U-tube manometer to measure the difference directly. Although this pressure difference is small, it can induce large axial velocities. In fact, by using the Bernoulli equation, $w = [(2/\rho)\Delta p]^{1/2}$, to calculate the upper limit on the induced velocity, a velocity of the same order as the local tangential velocity is obtained. Included in Fig. 22 is the pressure profile for an isothermal vortex with a potential velocity distribution ($v_\theta r^{-1}$) given by

$$\frac{p}{p_w} = \exp\left\{\frac{v_w^2 r_w^2}{2RT}\left[1 - \left(\frac{r_w}{r}\right)^2\right]\right\} \qquad (10)$$

It is interesting to note that for an isothermal process the static pressure goes to zero at the vortex centerline, whereas it can easily be shown that for an isentropic process the pressure goes to zero at a finite radius. The tangential Mach number distribution for an isothermal vortex with a potential velocity distribution is also shown in the Figure, for comparison with the experiment. For convenience, these theoretical distributions were matched arbitrarily to the measured static pressure ratio and tangential Mach number at the cylindrical wall ($r/r_w = 1$). This may not be the most realistic match point, since a large part of the flow adjacent to the cylindrical wall should be greatly affected by the presence of the concave wall and the driving jets. However, it is by no means clear at this time what the nature of these effects are, and at what radius they become insignificant. It is believed

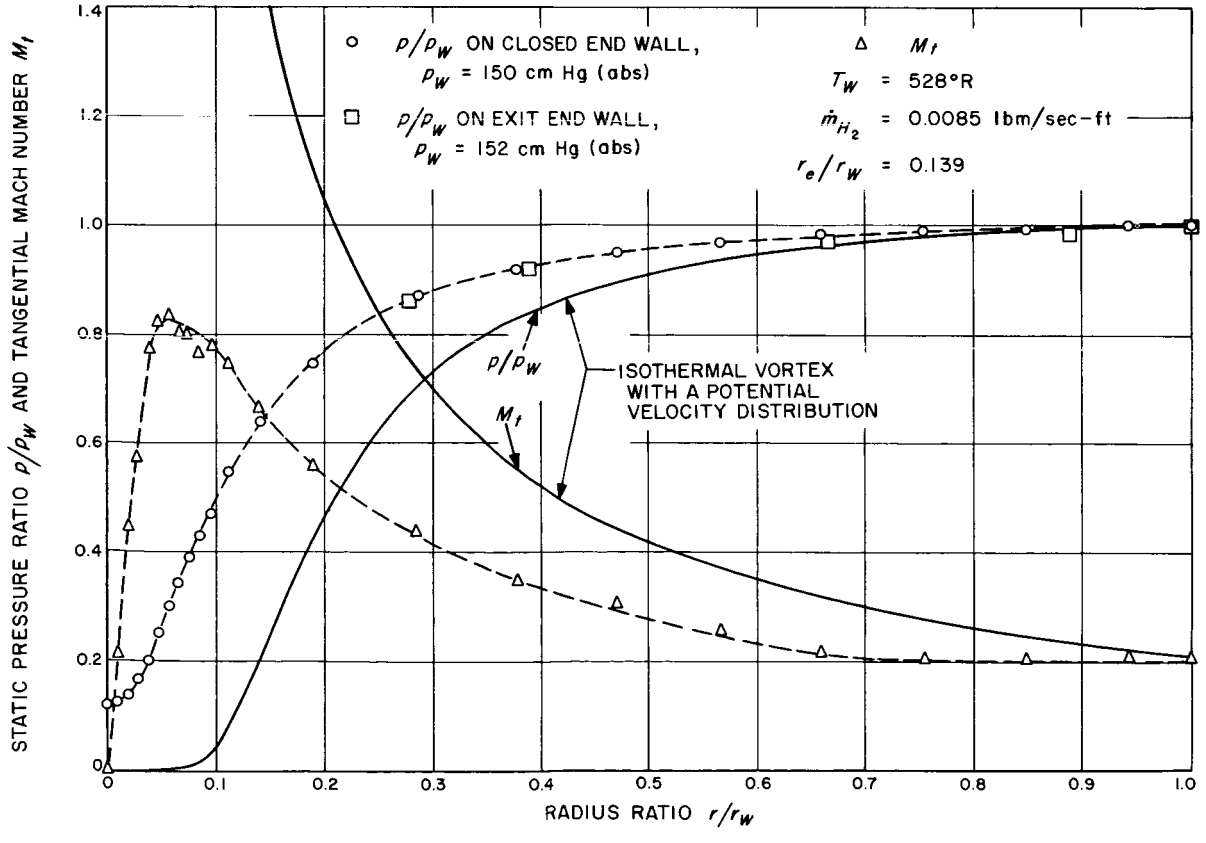

Fig. 22. Radial static pressure and tangential Mach number distributions for a medium-strength vortex

that the remaining difference between the theoretical and experimental distributions is due to viscous shear, turbulence, and the axial flows induced by the end-wall boundary layers.

The radial static pressure distribution along the closed end wall was also determined with the sampling probe located at 1.35, 2.68, 4.02, and 5.20 vortex tube diameters from the closed end wall. With the probe at $Z/D=1.35$, 2.68, and 4.02, the pressure on the centerline was above that shown in Fig. 22 by approximately 1 cm Hg, but the profiles were essentially the same at radius ratios greater than 0.025. With the probe at $Z/D=5.20$, the centerline pressure was above that shown in the Figure by 4.0 cm Hg, and the two profiles were the same at radius ratios greater than 0.050. Therefore the axial position of the sampling probe has only a small effect on the radial static pressure distribution as measured on the closed end wall. However, these small pressure changes could result in large variations of the axial velocity in the vicinity of the centerline.

b. Variation of density ratio distributions with axial position. For the same vortex tube configuration and cylindrical wall static pressure and approximately the same mass flow rates of hydrogen and Freon-13, the radial distribution of the heavy to light gas mass density ratio was measured at the five axial positions stated previously. These distributions are shown in Fig. 23, normalized with respect to the mass density ratio in the vortex tube manifold. This ratio of mass densities in the vortex tube manifold is equal to the ratio of heavy to light gas mass flow rates of the injected homogeneous mixture.

The most striking difference in the distributions is the change in both the maximum and minimum density ratio as a function of axial position. It is well known that a major portion of the fluid injected into the vortex is drawn into the boundary layer on the vortex tube end walls and is then accelerated radially inward by the free-stream radial pressure gradient that is impressed on the boundary layer. On the closed end wall, this boundary layer fluid must eventually erupt from the surface near the centerline and flow axially down the tube. It is believed that this flow, which originates at the larger radii, brings to the core of the vortex a concentration ratio that is not much greater than that of the manifold since it probably flows radially through the high pressure gradient too fast for the generated diffusion rate to have a significant effect on its relative concentration. This erupting boundary layer fluid might then dilute the mixture at radii of maximum heavy gas concentration in radial planes near the closed end wall and enrich the would-be low concentration near the center of these same planes. As this fluid, which flowed through the boundary layer along the closed end wall, flows axially down the tube, its heavy gas concentration is probably altered by the radial pressure gradient. That is, the strong positive radial pressure gradient and the weak positive concentration gradient found in planes near the closed end wall would induce an outward radial diffusion velocity of the heavy species. This is suggested by the expression for the heavy gas diffusion velocity, $\bar{u}_H$, simplified for this problem where the density ratio is much less than one and is given by

$$\bar{u}_H = D_{LH}\left[\left(\frac{m_H}{m_L}-1\right)\frac{d}{dr}\ln p - \frac{d}{dr}\ln\frac{\rho_H}{\rho_L}\right] \quad (11)$$

D_{LH} is the binary diffusion coefficient, m_H and m_L the molecular weight of the heavy and light species respectively, p the sum of the heavy and light gas partial pressures, and ρ_H and ρ_L the mass densities of the heavy and and light species, respectively. This diffusion velocity is relative to the mass average radial velocity. Now the radial component of the heavy gas mass flow rate per unit length can be written as

$$\dot{m}_H = 2\pi r\rho_H(u_0+\bar{u}_H) \quad (12)$$

The variable u_0 is the mass average radial velocity of the binary mixture; however, since the heavy gas density is much less than that of the light gas, u_0 is approximately equal to the radial velocity of the hydrogen. Throughout most of this axial core flow, here defined as that fluid which erupted from the end-wall boundary layer, the radial velocity of the hydrogen is probably zero, or very nearly zero, which means that the heavy gas diffusion velocity will cause a net flow of the heavy species radially out of this core as the fluid mixture flows along the vortex tube centerline. This net radial outflow will continue until a radius is reached at which the inward mass average radial velocity just equals the heavy gas diffusion velocity. Outside this radius ratio the inward radial mass average velocity u_0 is probably greater in magnitude than the heavy gas diffusion velocity, resulting in a net inward flow of heavy gas. The result of this entire flow and diffusion process could be a maximum concentration at approximately this critical radius and the observed increasing maximum and decreasing minimum concentration as the core fluid flows down the tube. As this fluid flows along the centerline, the positive density ratio gradient inside the peak concentration point becomes greater and since it counteracts the effect of the radial pressure gradient, an equilibrium might be reached between these two effects, resulting in a zero diffusion

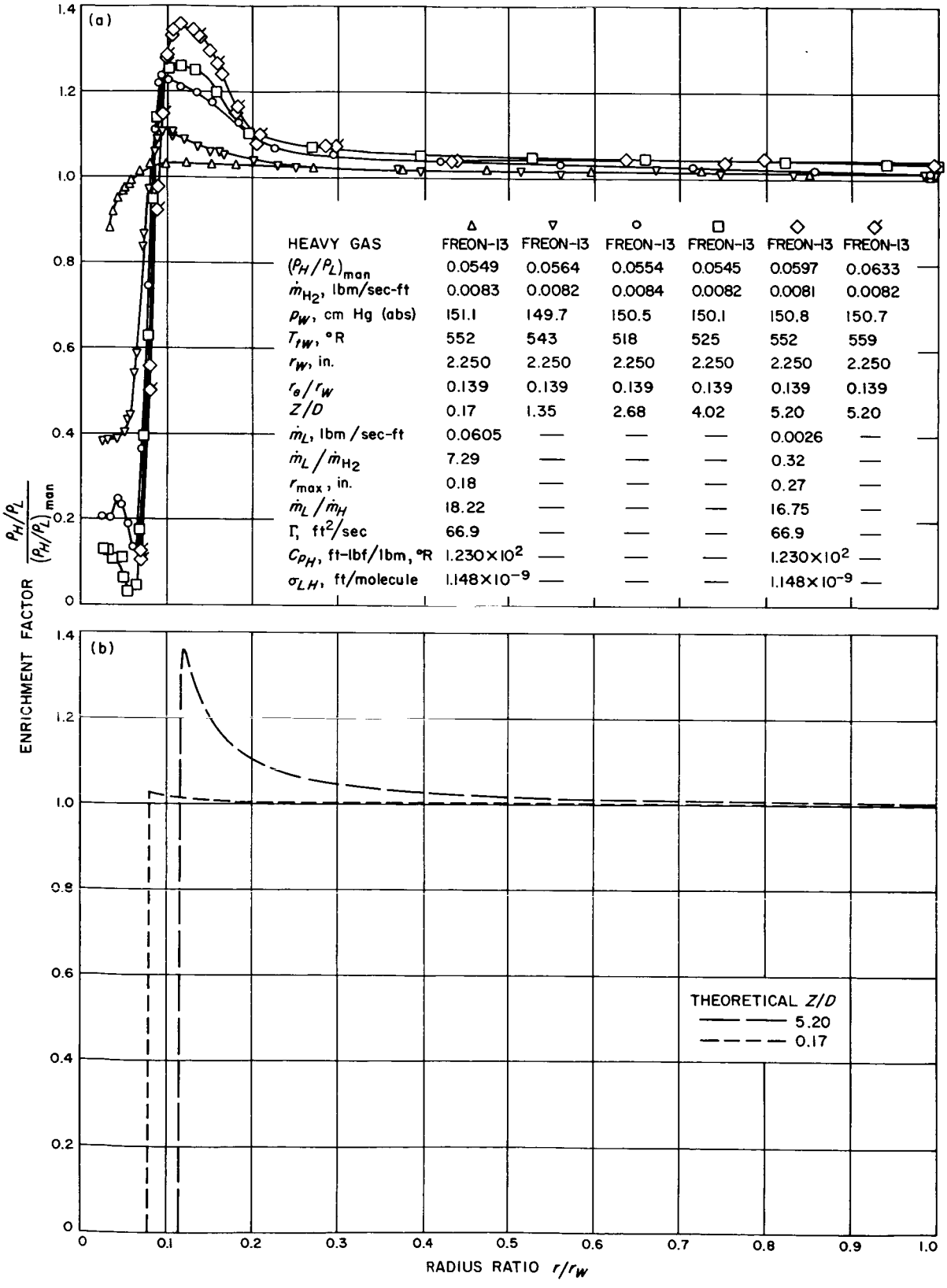

Fig. 23. Axial variations of the density ratio

velocity at some point downstream of the closed end wall. It appears that such an equilibrium may not have been reached in the 24-in.-long vortex tube used in the experiment shown in Fig. 23 since the density ratio at, for example, a radius ratio of 0.07, appears to be still decreasing between $Z/D=4.02$ and 5.20. If this flow and diffusion model is correct, no such equilibrium should exist outside the peak concentration point since the heavy gas should be diffusing uniformly into the region of maximum concentration from the free stream along the length of the vortex tube.

Besides the core flow described above, two other regions of strong axial flow have been observed in an incompressible vortex-type flow similar to the type used in these separation experiments (Ref. 3). The core flow in Ref. 3 was designated *A* and a second axial flow, designated *B*, was found to originate at the boundary layer on the end wall containing the exit hole. This flow surrounded the core and flowed axially in the opposite direction, penetrating the full length of the vortex tube. It was also observed that this flow occurred just outside the exit-hole radius for all diameters used. As this axial flow reached the closed end wall it split, with a part flowing radially inward and merging with the core, and the remainder flowing radially outward and merging with the third observed axial flow *C*. This third flow originated at the closed end-wall boundary layer at large radii, and flowed just outside and in the opposite direction to *B*, losing its identity as it approached the end wall containing the exit hole. For a detailed diagram of this complicated flow structure, see Ref. 3. If these counter flows had been present in the experiments of Fig. 23 they would have been found at a radius ratio greater than approximately 0.15, according to the results of Ref. 3, and hence would have occurred in regions of almost uniform density ratio. Therefore they probably could not have a significant effect on the density ratio distributions in the same way as does the core flow. However, they could affect the distributions indirectly since their occurrence probably does have an effect on the basic flow field and pressure gradient distribution.

Two analytic density ratio distributions were computed for conditions corresponding with the experiments made at $Z/D = 0.17$ and 5.20 of Fig. 23; they are also shown in this figure. The relatively large light gas mass flow rate $\dot{m}_L$, computed for the experiment at $Z/D = 0.17$, is due to the small r_{max} assumed for the computations. The general result, that the theoretical profiles are narrower than the experimental results and that the theoretical density ratio does not increase again at small radii as do those of the experiments, is again apparent. The experimental density ratio increase at small radii is probably due to the viscous core flow, which has been discussed, and if so could not be predicted with the present two-dimensional inviscid theory. The minimum density ratio and the maximum tangential Mach number occur at approximately the same radius. Inside this radius the radial pressure gradient decreases rapidly, resulting in a lower diffusion velocity and hence a higher density ratio in this part of the core flow.

To help clarify this complex flow, the heavy gas diffusion velocity has been computed from the experimental data by using the following equation for the heavy gas diffusion velocity in a binary gaseous mixture:

$$\bar{u}_H = \frac{D_{LH}}{r_W}\left[\frac{\left(\frac{m_H}{m_L}-1\right)\left(\frac{\rho_H}{\rho_L}+\frac{m_H}{m_L}\right)}{m_H/m_L\,(\rho_H/\rho_L+1)^2}\frac{d}{d\,r/r_W}\ln\frac{p}{p_W} - \frac{1}{(\rho_H/\rho_L+1)}\frac{d\ln\rho_H/\rho_L}{d\,r/r_W}\right] \tag{13}$$

This equation has been normalized with respect to a reference radius r_W taken as the experimental vortex tube radius, and the static pressure p_W measured at the vortex tube cylindrical wall. Notice that for these experiments, in which $\rho_H/\rho_L \ll 1$, Eq. (11) normalized with respect to p_W and r_W could have been used with very little error since Eq. (11) is a simplified form of the more general Eq. (13).

The radial distribution of the pressure gradient

$$\frac{d}{dr/r_W}\ln\frac{p}{p_W}$$

was obtained by graphically differentiating the pressure distribution of Fig. 22 and dividing the results by p/p_W. This distribution is shown in Fig. 24, together with a theoretical distribution computed from the radial momentum equation, and the energy equation written for a binary potential vortex flow:

$$\frac{d}{dr/r_W}\ln\frac{p}{p_W} = \frac{m_H\,\Gamma^2}{k\,g_c}\left(\frac{1+\rho_H/\rho_L}{m_H/m_L+\rho_H/\rho_L}\right)\frac{r_W}{r^3T} \tag{14}$$

$$T = T_\infty - \frac{(\dot{m}_H/\dot{m}_L+1)\,\Gamma^2\,r^{-2}}{2\,g_c\,C_{p_L}\left(\frac{\dot{m}_H}{\dot{m}_L}\frac{C_{p_H}}{C_{p_L}}+1\right)} \tag{15}$$

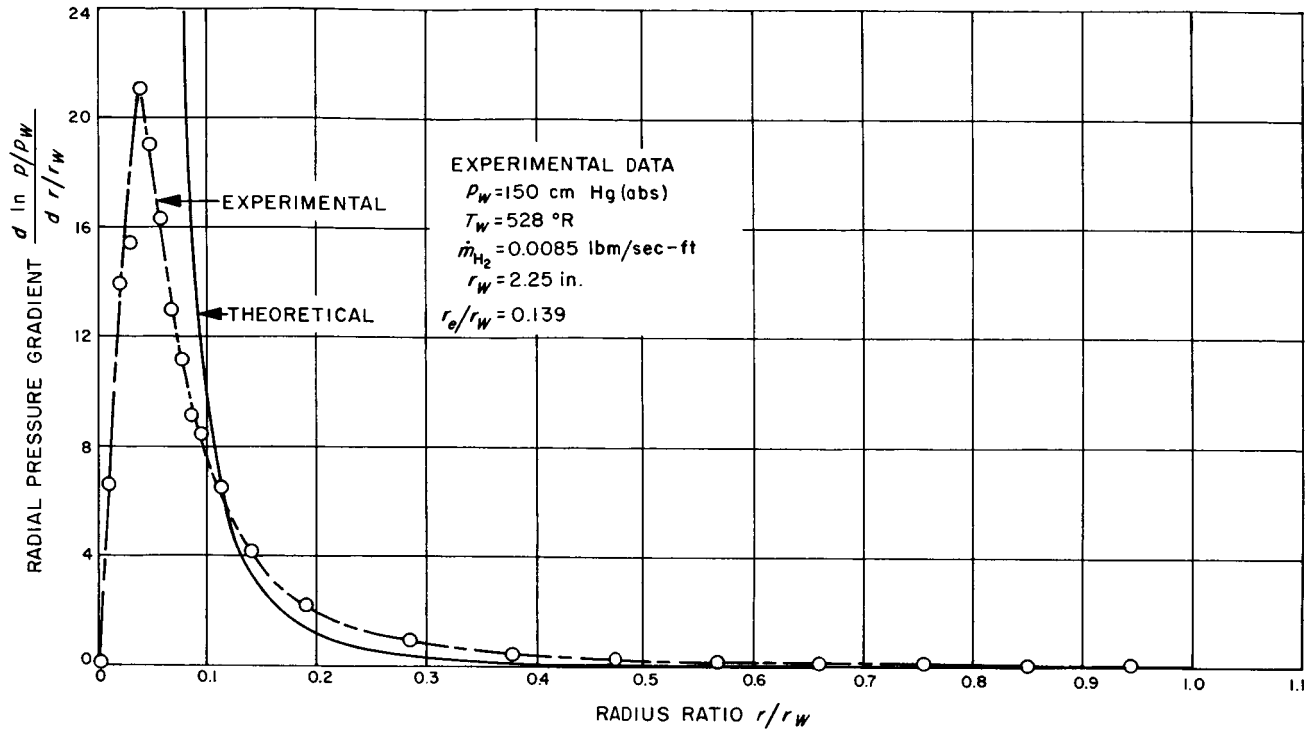

Fig. 24. Radial distribution of the radial pressure gradient for a medium-strength vortex

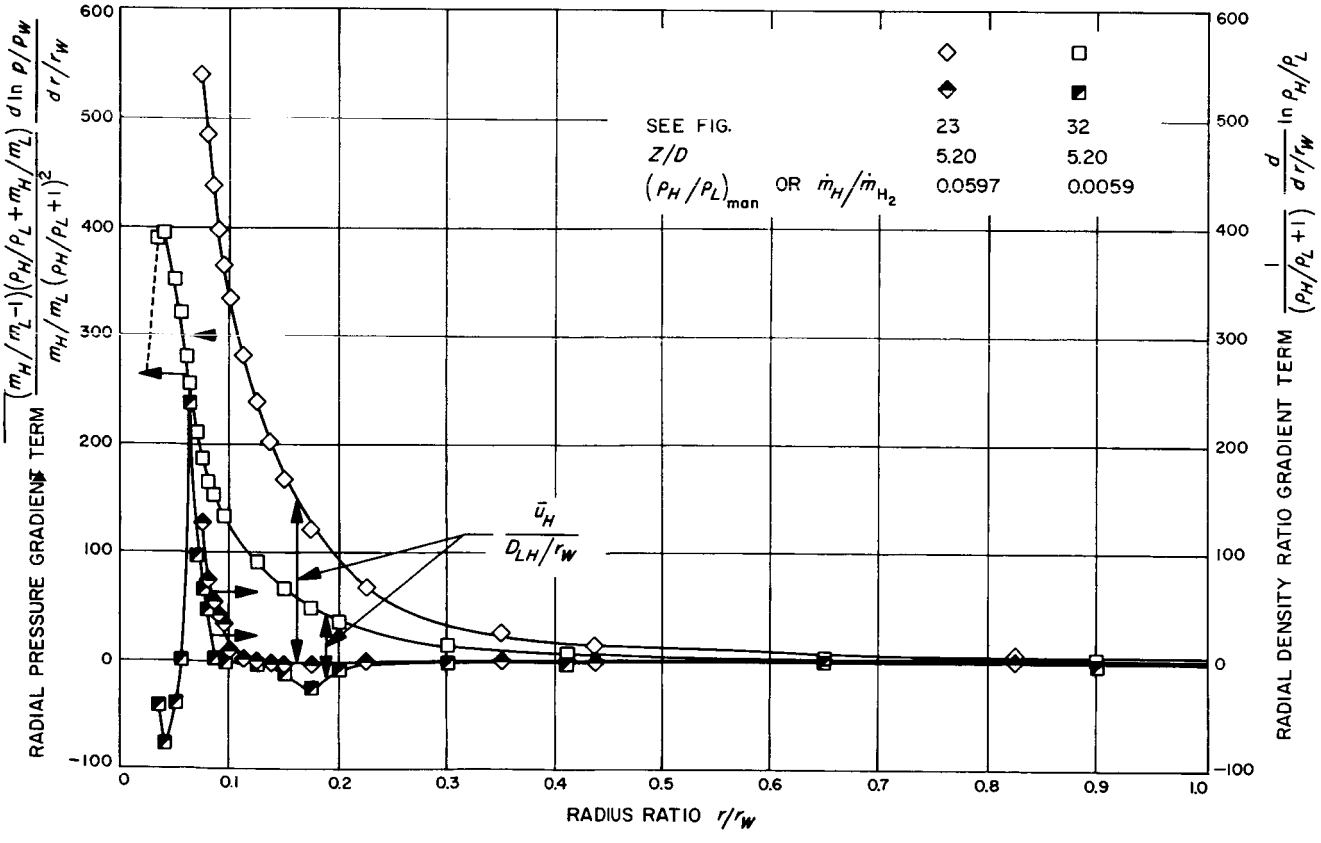

Fig. 25. Radial distribution of the terms involved in the diffusion velocity equation

For the theoretical distribution of Fig. 24, the density ratio distribution and ratio of mass flow rates of Fig. 23 ($Z/D = 5.20$) was used and Γ was chosen so that the theoretical pressure gradient equaled the experimental value at the radius at which the density ratio was a maximum.

The pressure gradient term of Eq. (13), corresponding to the density ratio distribution of Fig. 23 ($Z/D = 5.20$) and experimental pressure gradient distribution of Fig. 24, is represented by the open diamond symbol in Fig. 25. The density ratio gradient term of Eq. (13), obtained by graphically differentiating the distribution at $Z/D = 5.20$ in Fig. 23, is also shown in Fig. 25 by the half-closed diamond symbol. The difference between these two distributions is the nondimensional heavy gas diffusion velocity $\bar{u}_H/(D_{LH}/r_W)$. The density ratio gradient has very little influence on the diffusion velocity for radii greater than r_{max}, and for radii less than r_{max} it subtracts from the pressure gradient term by as much as 20%.

The radial distribution of this nondimensional diffusion velocity has been determined for three of the experiments shown in Fig. 23 and is represented in Fig. 26 by triangles ($Z/D = 0.17$), circles ($Z/D = 2.68$), and diamonds ($Z/D = 5.20$). It is apparent that the slope

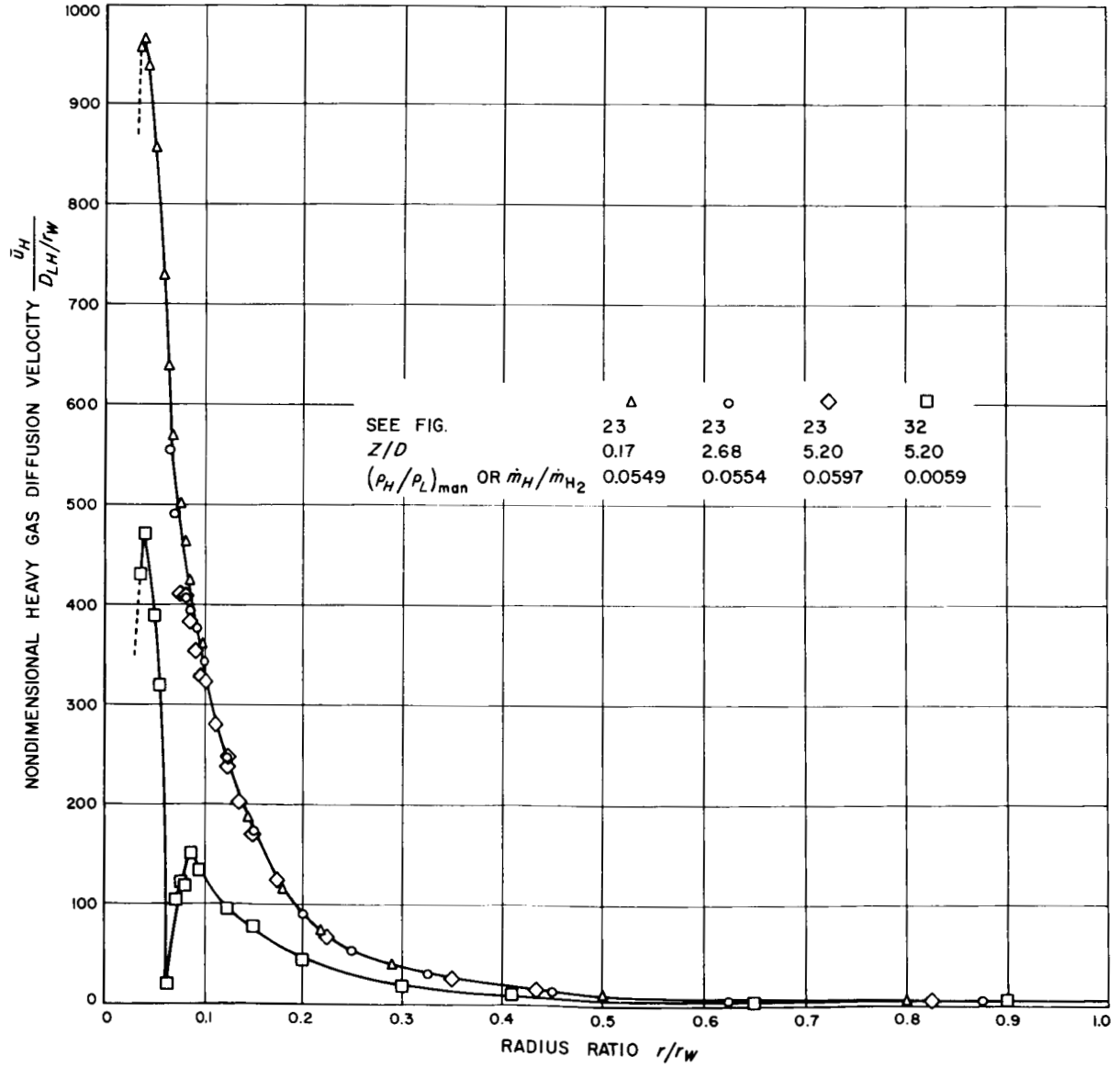

Fig. 26. Radial distributions of the nondimensional diffusion velocity

and level of the experimental density ratio distributions have only a small influence on the diffusion velocity; hence this velocity is caused primarily by the radial pressure gradient. It is believed that the static pressure measurements of Fig. 22 are representative of the entire flow field; hence the values in Fig. 26 should be reasonably accurate, provided that the flow is laminar, or, if it is turbulent, that the effects of turbulence can be represented by a modified D_{LH}. The influence of this diffusion velocity on the flow of heavy gas is dependent on the radial mass average velocity u_0 as shown by Eq. (12); however, the radial distribution of u_0 is unknown except for the idealized two-dimensional model.

By estimating the binary diffusion coefficient D_{LH} by the methods of Ref. 11, some idea of the magnitude of the heavy gas diffusion velocity in a laminar flow can be obtained. This calculation, made for the three distributions of $\bar{u}_H/(D_{LH}/r_W)$ previously discussed and shown in Fig. 26, is shown in Fig. 27. By assuming the flow to be isothermal and $\rho_H/\rho_L \ll 1$, the radial distribution of the mass average velocity u_0 was computed and is also shown in Fig. 27. This is an upper limit on u_0 since the computation is based on a two-dimensional vortex in which the mass flow rates are constant with radius. In a real vortex tube u_0 would be less than this for $r < r_W$ and would probably have a different radial distribution. In fact, the radial variations of ρ_H/ρ_L, found experimentally, are an indication that the actual u_0 is much smaller than that shown in Fig. 27, for if the generated diffusion velocities are to have a measurable effect on the binary flow, u_0 must be of the same order as $\bar{u}_H$ (Eq. 12). Also, since the diffusion velocity is relative to the mass average velocity, the algebraic sum of these two velocities gives the absolute radial velocity of the species u_H. Fig. 27 shows this velocity to be everywhere negative or inward. If the heavy gas is to flow radially outward, as it is believed to do in the core, $|u_0|$ must be less than $\bar{u}_H$, or u_0 must itself be positive or outward. Hence, the actual radial flow of hydrogen in a real vortex tube is much less than what would occur if the flow were truly two-dimensional.

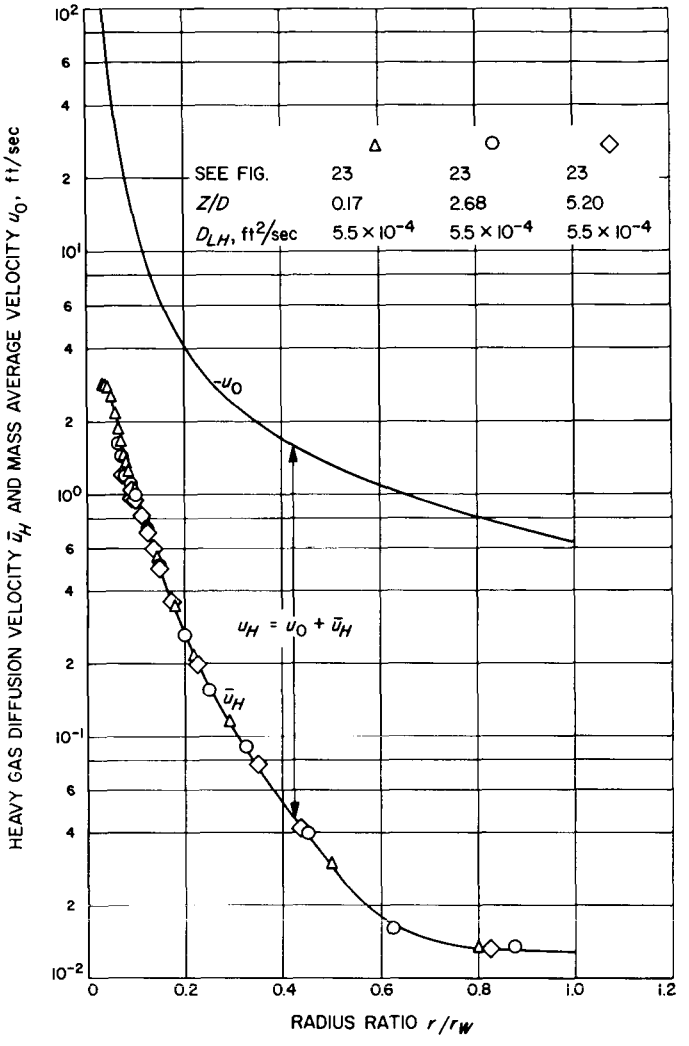

Fig. 27. Radial distribution of the diffusion and mass average velocity

c. Effect of mass flow rate ratio $\dot{m}_H/\dot{m}_L$. For the same cylindrical wall static pressure, vortex tube configuration, and hydrogen mass flow rate, the radial distribution of the heavy to light gas mass density ratio was measured at the station nearest the end wall containing the exit hole ($Z/D = 5.20$) for two mass flow rates of Freon-13 (Fig. 28), and two mass flow rates of argon (Fig. 29). Both figures again demonstrate that the enrichment factor $(\rho_H/\rho_L)/(\rho_H/\rho_L)_{\text{man}}$ increases when there is a decrease in the density ratio in the vortex tube manifold or the ratio of heavy to light gas mass flow rates. This phenomenon is probably due, in part, to the fact that the heavy gas diffusion velocity increases as the level of the heavy gas density is decreased for radii greater than $r_{\max}$, as suggested by Eq. (13). Also, in the discussion of Fig. 23 it was postulated that the mass average velocity for radii less than that of the peak density ratio $r_{\max}$ is insignificantly small, so that the diffusion velocity is the absolute outward heavy gas velocity. In this region of the vortex the density ratio gradient term is positive; therefore, as it increases because of the decreased density ratio level as suggested by Eq. (13), the outward heavy gas velocity decreases, causing the observed increase of the density ratio for radii less than $r_{\max}$. In both Figs. 28 and 29, the

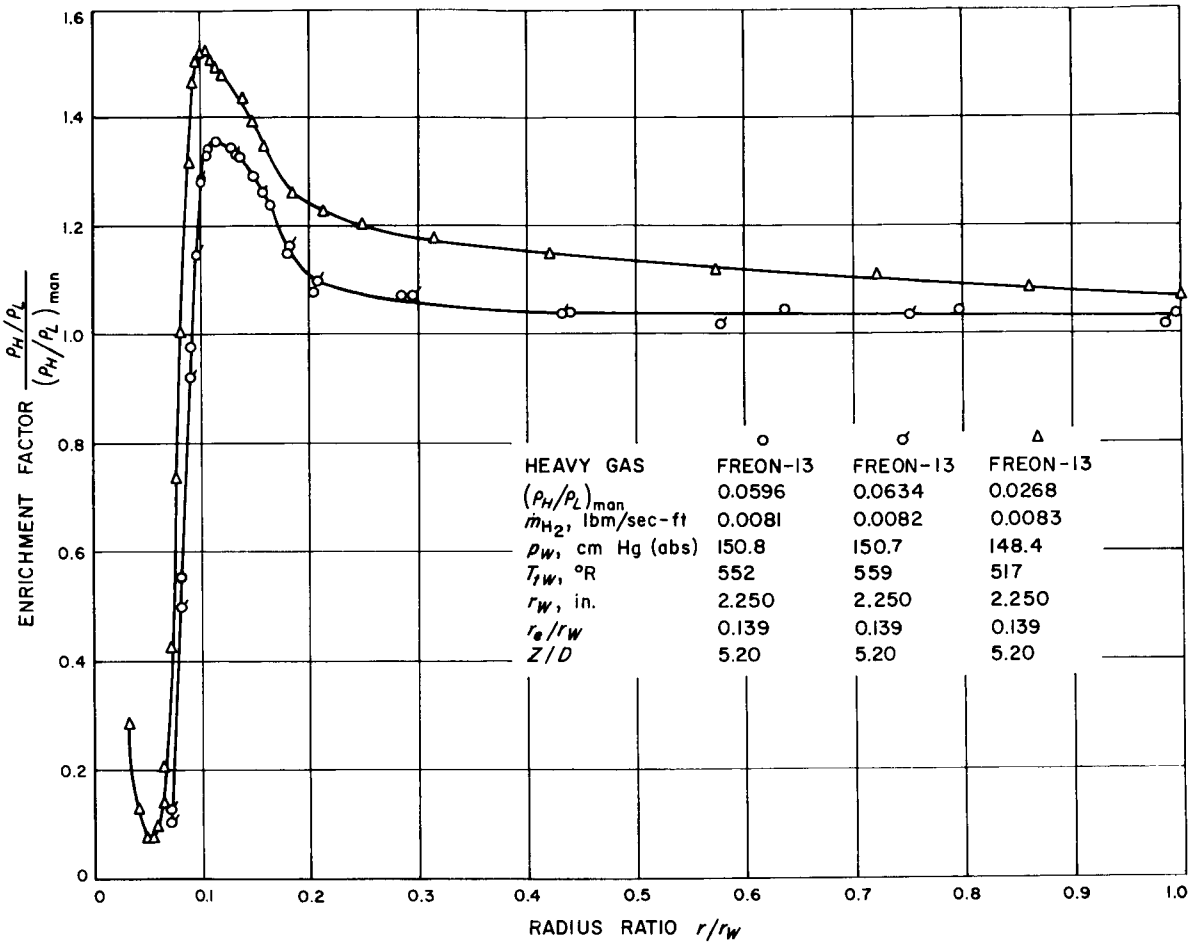

Fig. 28. Effect of Freon-13 mass flow rate on the density ratio distribution

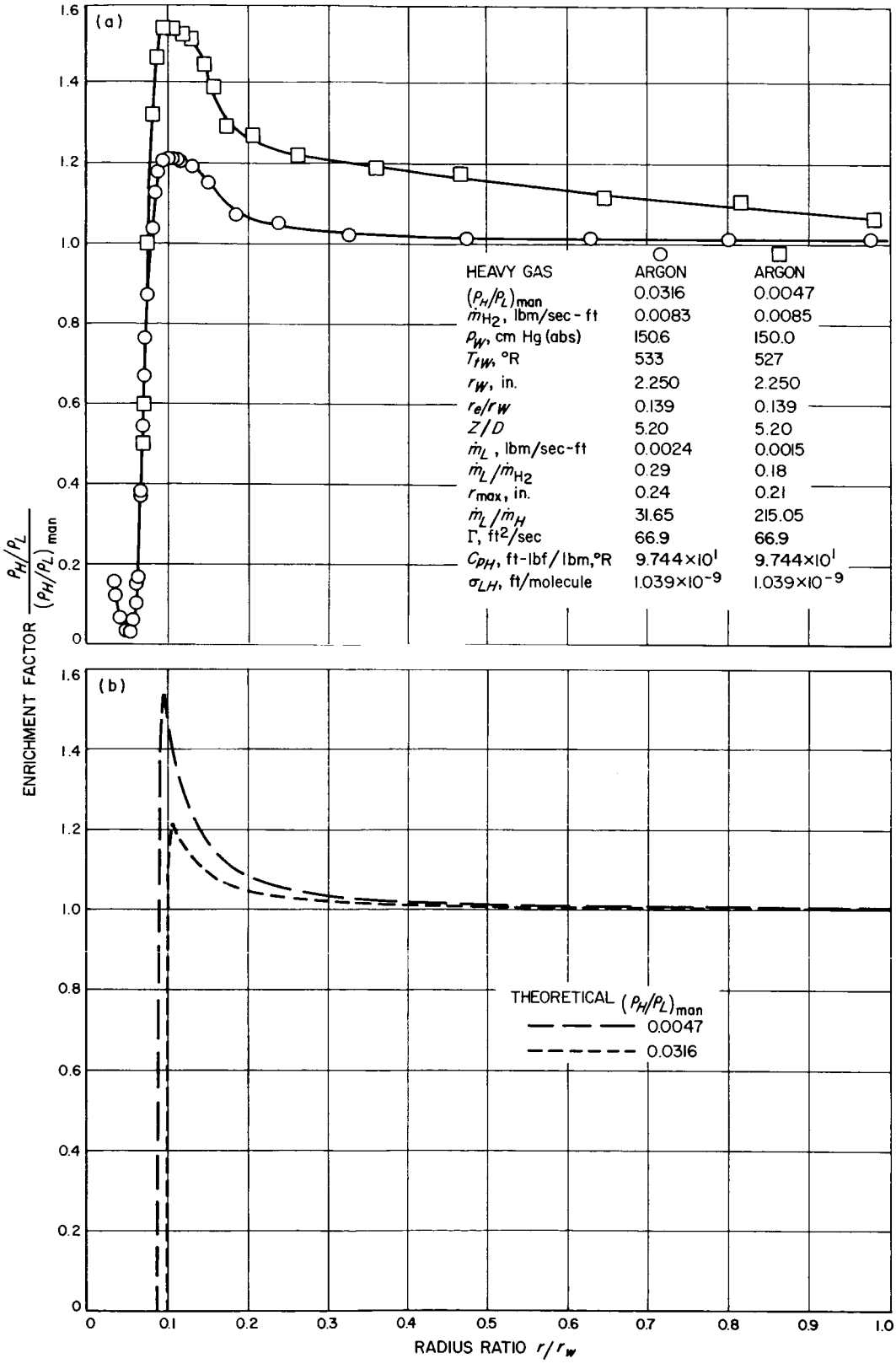

Fig. 29. Effect of argon mass flow rate on the density ratio distribution

radius at which the density ratio profile reaches a maximum r_{max} appears to decrease as the ratio of mass flow rates $\dot{m}_H/\dot{m}_L$ decreases. However, by computing the theoretical light gas mass flow rate $\dot{m}_L$ for the experiments of Fig. 29, it was found that the measured shift of r_{max} was still not enough to satisfy Eq. (9). This may be an indication that the sampling probe obscures the true location of the maximum density ratio.

d. Effect of heavy gas molecular weight m_H. Again, for the same vortex tube configuration, cylindrical wall static pressure, and hydrogen mass flow rate, the radial distribution of the heavy to light gas mass density ratio was measured at the station nearest the exit hole ($Z/D = 5.20$) for three different heavy gases. The gases used were argon with a molecular weight of 39.94, Freon-13 with a molecular weight of 104.47, and perfluoropropane (C_3F_8) with a molecular weight of 188.03. The results are shown in Fig. 30. Because the ratio of heavy to light gas mass flow rate varied from 2.7 to 4.1%, it is not possible to ascribe the differences in enrichment factor between the three distributions to molecular weight only. However, comparing the distribution for argon with that for C_3F_8, one can conclude that the enrichment factor does increase as the heavy gas molecular weight increases, since if the ratio of mass flow rates for the argon experiment were increased to 4.1% or that of the C_3F_8 decreased to 3.2%, these two distributions would be even further separated, according to the results of Figs. 28 and 29. Also, there appears to be a tendency for the distributions to have a sharper peak in the region of maximum density ratio as the heavy gas molecular weight increases.

e. Effect of light gas molecular weight $\dot{m}_L$. With the sampling probe at 4.02 vortex tube diameters from the closed end wall, the radial distribution of the heavy to

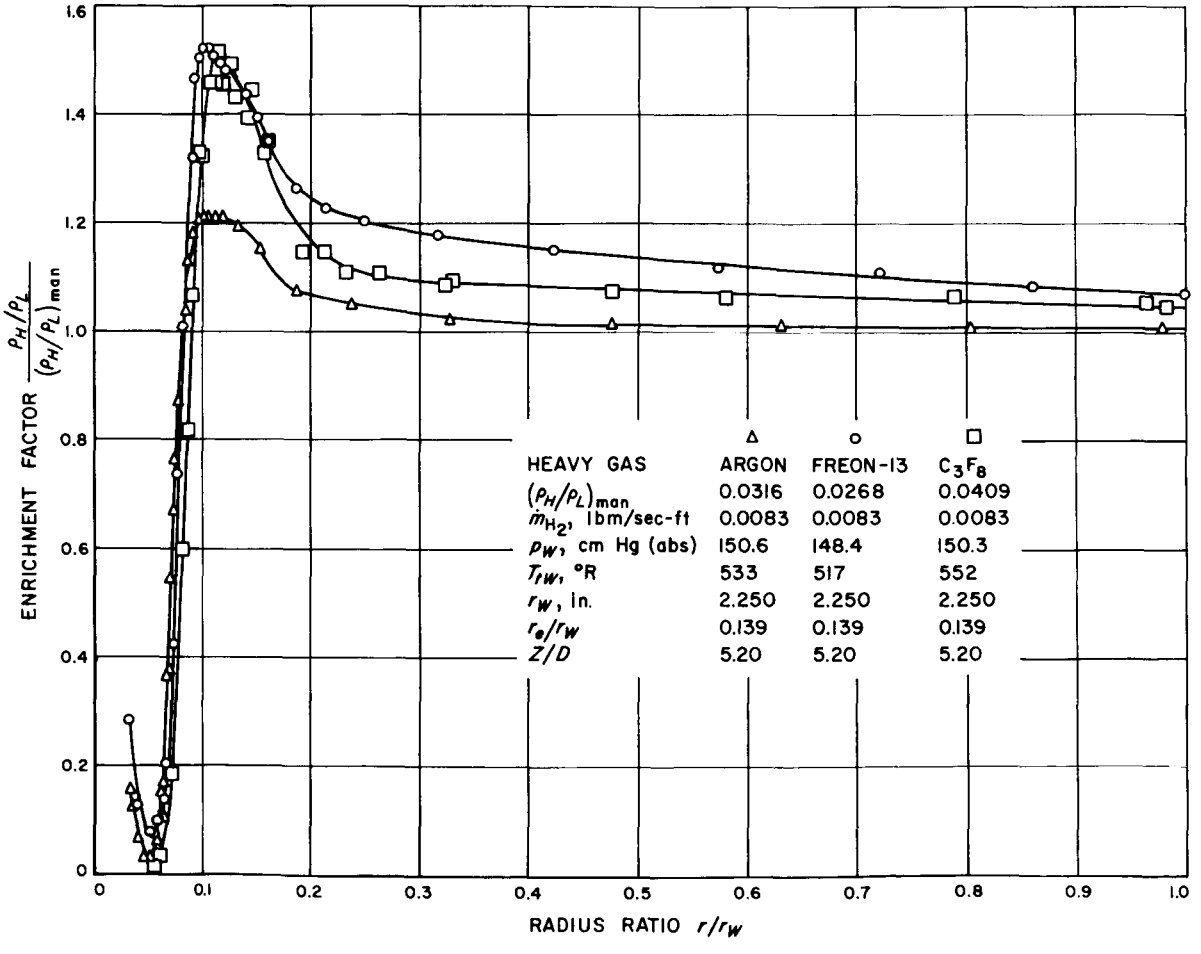

Fig. 30. Effect of heavy gas molecular weight on the density ratio distribution

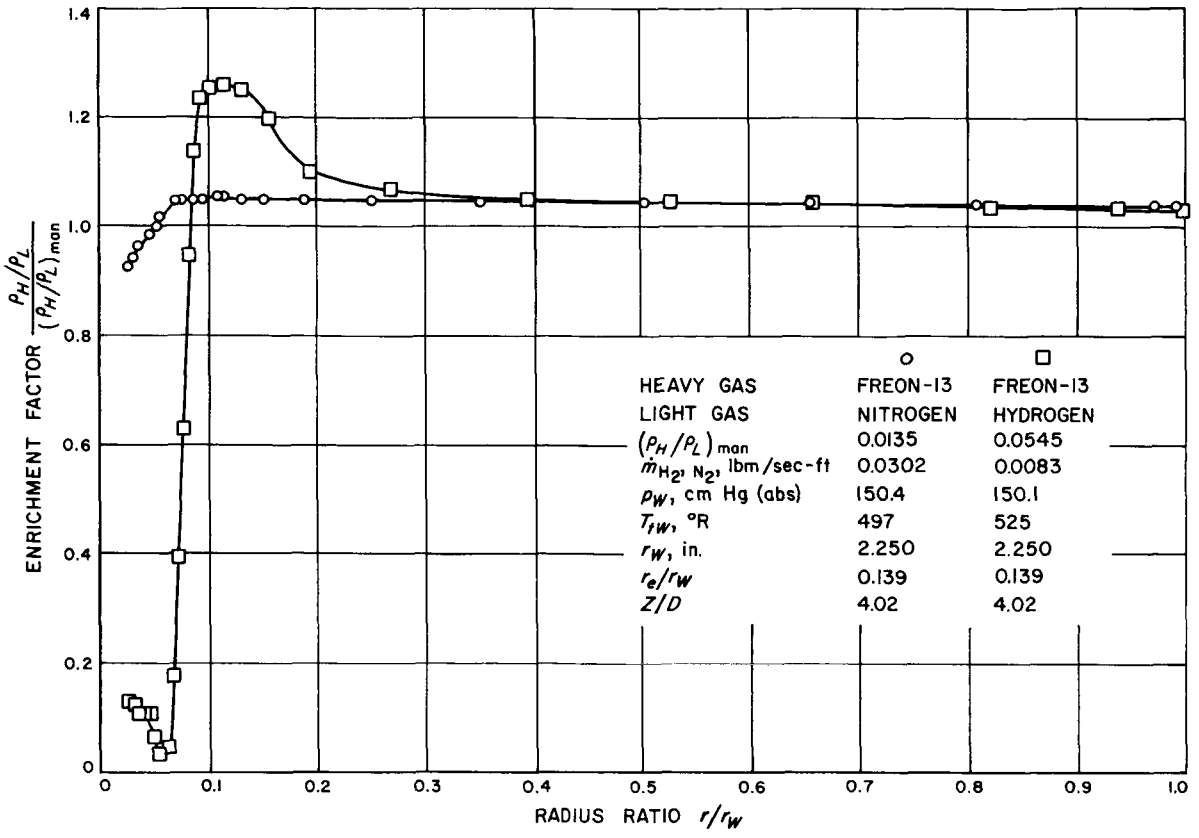

Fig. 31. Effect of light gas molecular weight on the density ratio distribution

light gas mass density ratio was measured for a mixture of nitrogen and Freon-13. The results are shown in Fig. 31, together with a distribution made with a hydrogen–Freon-13 mixture at the same cylindrical wall static pressure and approximately the same Freon-13 mass flow rate. In order to maintain the same cylindrical wall static pressure and hence the same radial static pressure distribution with the same configuration, the nitrogen mass flow rate had to be greater than that of the hydrogen experiment. This made the heavy to light gas density ratio in the vortex tube manifold for the nitrogen experiment less than that of the hydrogen experiment; hence the density ratio level of the two experiments should not be compared. However, the lack of a definite peak in the density ratio distribution and the higher relative density ratio level near the vortex tube centerline for the nitrogen case demonstrate the effect that the much higher nitrogen molecular weight has on the diffusion process. The fact that the Freon–nitrogen density ratio is 4 to 5% higher than the manifold value at large radii was not expected because the low molecular weight ratio of the Freon-13–nitrogen mixture makes the pressure gradient term in Eq. (13) small. Possibly an error was made in measuring the manifold density ratio.

f. Effect of injecting heavy gas directly into the vortex tube. All the separation experiments discussed so far were made by premixing the light and heavy gases and injecting the uniform mixture into the vortex tube through the driving jets. A second type of separation experiment was performed in which pure hydrogen was injected through the driving jets and the heavy gas was added to the system through an orifice at the center of the closed end wall. The purpose was to inject the heavy gas directly into the core flow discussed above (Subsection 2, Part b). The heavy gas injector is shown in Fig. 3. The heavy gas was injected into the vortex from a 0.238-in.-D cylindrical hole located at the center of the closed end wall. It emerged with a swirl component of unknown strength in the same direction as that of the external vortex. The results of two experiments made with this injector, in which argon was the heavy gas, are indicated by the circles and squares in Fig. 32. The results of a third experiment, to be discussed subsequently, are also shown in this figure and are indicated by triangles. These results are presented as the heavy to light gas density ratio normalized with respect to the heavy to light gas mass flow rate since the density ratio in the vortex tube manifold was zero at all times. However, because of the

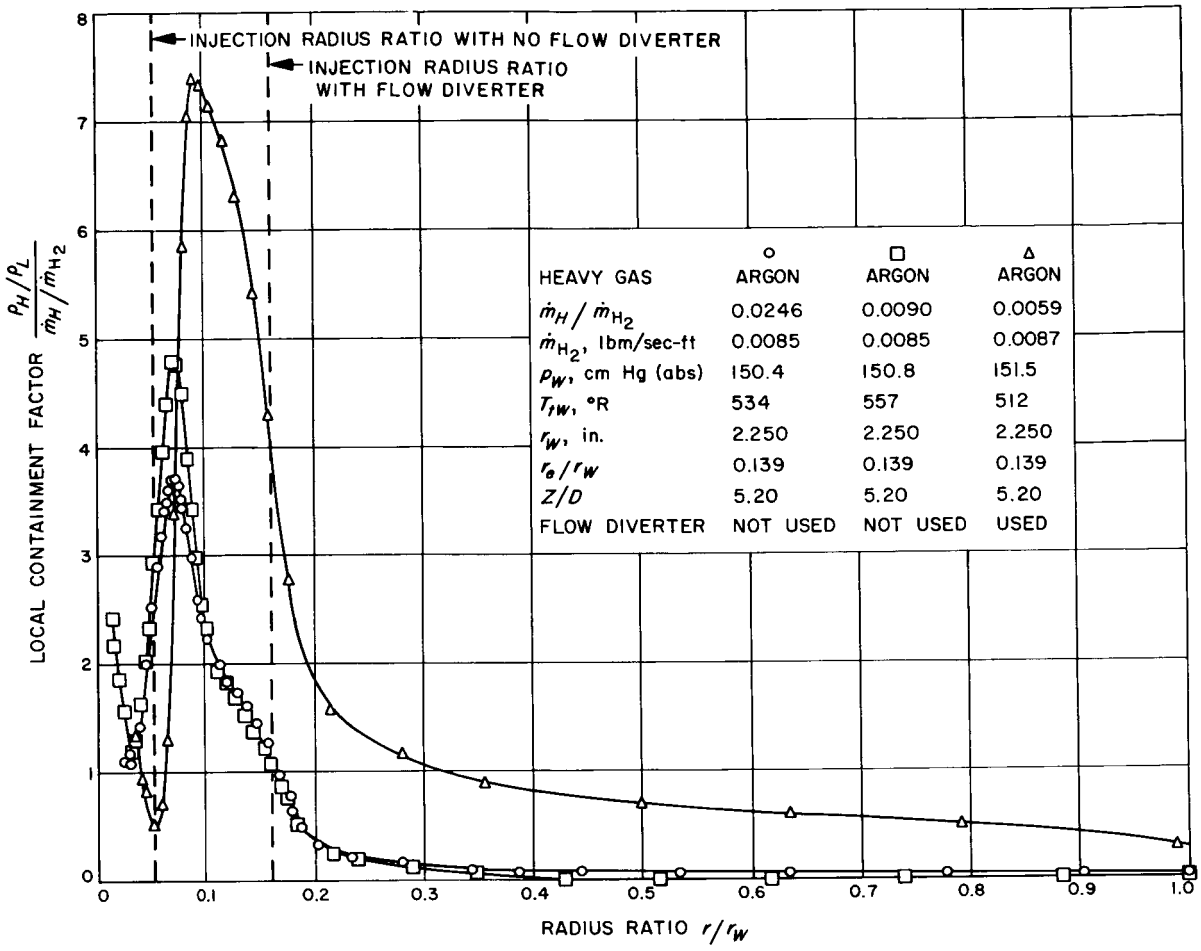

Fig. 32. Results of injecting argon directly into a vortex

equivalence between the ratio of mass flow rates and the ratio of densities in the manifold for a uniform mixture, the results in Fig. 32 can be compared with the other diffusion experiment results. In this Figure, the only difference between the two experiments now under discussion was the heavy gas mass flow rate, which was approximately 1% of the hydrogen mass flow rate in one experiment and 2.5% in the other. The variation in the heavy gas mass flow rate probably caused a variation in the heavy gas tangential and axial velocity at the point of injection. The experiments were performed at a station that was 5.20 vortex tube diameters from the point of heavy gas injection, and it was found that by the time the heavy gas reached this station, most of it had diffused outward to radii greater than the injection radius. In fact, for the higher flow rate experiment it appears that some heavy gas found its way to the vortex tube cylindrical wall. Note also the great similarity in the two distributions, differing only in magnitude at the radius of maximum density ratio and at large radii.

To reduce the heavy gas axial velocity at the point of injection, and also to promote mixing with the hydrogen in the end-wall boundary layer, a deflector plate was mounted as shown in Fig. 3. This deflector plate forced the heavy gas to spiral out to a radius ratio of 0.163 before blending with the hydrogen. The density ratio was again measured at a station that was 5.20 vortex tube diameters from the argon injection point for a heavy gas mass flow rate approximately 0.6% that of the hydrogen. This distribution is also shown in Fig. 32, indicated by triangles. In this case the maximum density ratio was found at a radius ratio less than that at which the heavy gas was injected. Also, with the reduced axial velocity, a considerable amount of heavy gas managed to find its way to the cylindrical wall, possibly indicating the existence of secondary currents.

With the deflector plate again in place, a second heavy gas, sulfur hexafluoride (SF_6), was used and the results were compared with those of a similar argon experiment

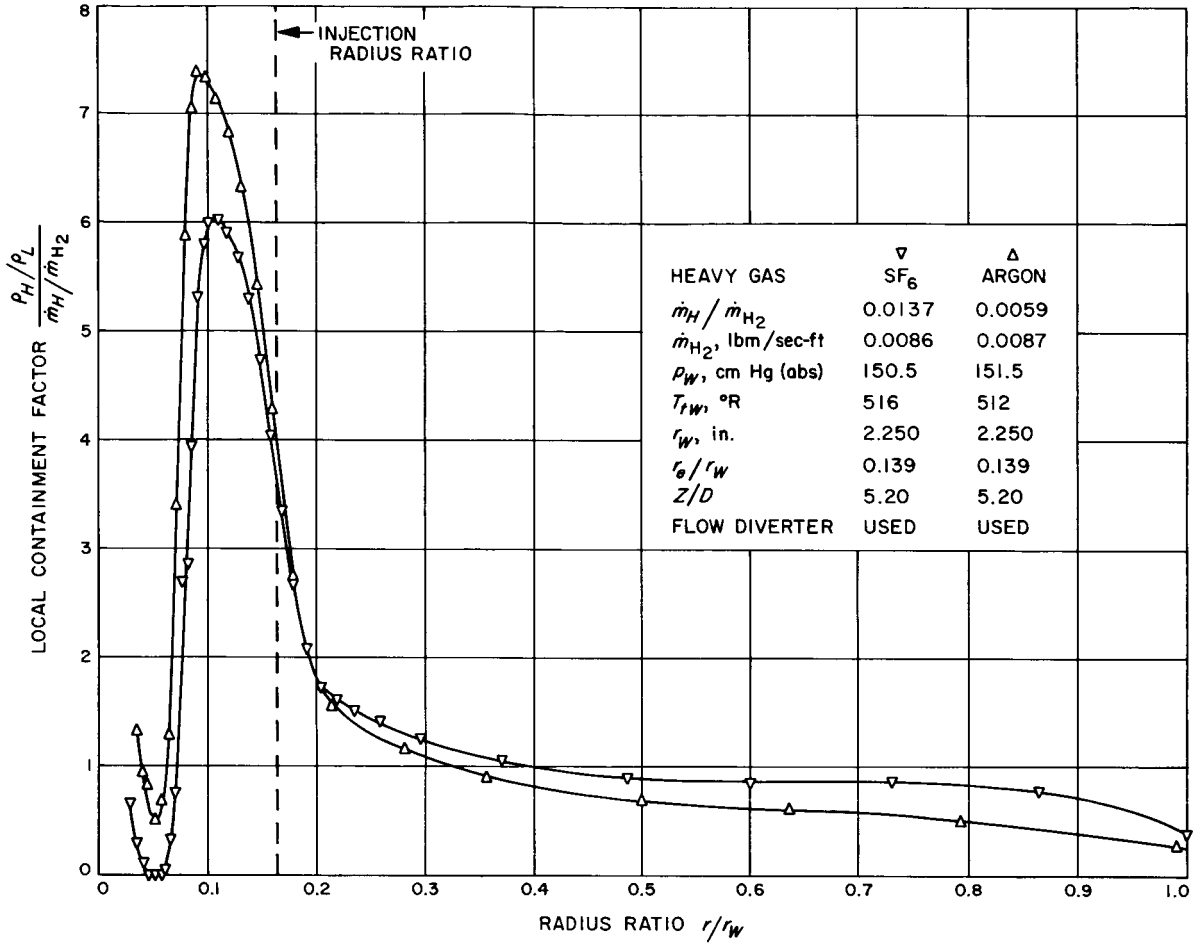

Fig. 33. Results of injecting sulfur hexafluoride directly into a vortex

(Fig. 33). A similarity between the two distributions is again evident, with the maximum and minimum density ratios occurring at approximately the same radii. In these experiments, the maximum density ratio was found at the same radius as in the experiments in which the two gases were premixed and the hydrogen mass flow rate was the same (Fig. 29). It is believed that this result reinforces the conviction that the density ratio distributions are primarily governed by the axial core flow, discussed previously, and not by the inward-flowing heavy gas assumed for the model of Ref. 1. The density ratio distributions in the region of the maximum density ratio display the same characteristic gradual increase to a maximum as the radius is reduced, followed by a relatively sharp decrease after the maximum is reached, which is evident in the experiments using premixed fluids.

As was done previously, the nondimensional heavy gas diffusion velocity for the experiment, represented by triangles in Fig. 32, was determined; the velocity is shown in Figs. 25 and 26 by square symbols. The pressure gradient term shown in Fig. 25 is approximately one-half that for the Freon-13 experiments because of the lighter heavy gas (argon) used in the experiment of Fig. 32. The density ratio term, also shown in Fig. 25, is negative over some portions of the vortex because of the high negative density ratio gradients. Because of the low heavy gas molecular weight and high density ratio gradients, the diffusion velocity approaches zero at one point (Fig. 26).

3. High-Strength Vortex ($\dot{m}_{H_2} = 0.022$ lbm/sec-ft)

a. Pressure and Mach number distribution. In order to further check the effect of hydrogen mass flow rate on the density ratio distributions, measurements were made for a light gas mass flow rate of 0.022 lbm/sec-ft. The vortex tube configuration was kept the same; therefore the cylindrical wall static pressure was increased from 150 to 370 cm Hg (abs). The exit gap δ was set at 0.096 in., providing an exit area of 0.45 in^2. The radial

distribution of static pressure on the closed end wall, made while the sampling probe was installed at a station that was 2.68 vortex tube diameters from the closed end wall, is shown in Fig. 34. Also shown is the radial distribution of tangential Mach number computed from the static pressure distribution.

b. Effect of heavy gas mass flow rates. Freon-13 was premixed with the hydrogen before injection, and the radial distribution of heavy to light gas density ratio was measured for five values of the manifold density ratio at a station that was 2.68 vortex tube diameters from the closed end wall. For these five experiments, the binary mixture was sampled at radii near the expected radius of maximum density ratio only; the results are shown in Fig. 35 and again demonstrate the effect of mass flow ratio on the maximum enrichment factor. The radial position of the maximum density ratio is the same as it was found to be in the experiments at which the cylindrical wall static pressure was 150 cm Hg (abs). There appears to be a slight shift of r_{max} toward the centerline as the mass flow ratio decreases. Again, by computing the theoretical light gas mass flow rate (Fig. 35), it is apparent that the observed small decrease of r_{max} is not large enough to account for the increase in the maximum enrichment factor with decreasing mass flow ratio.

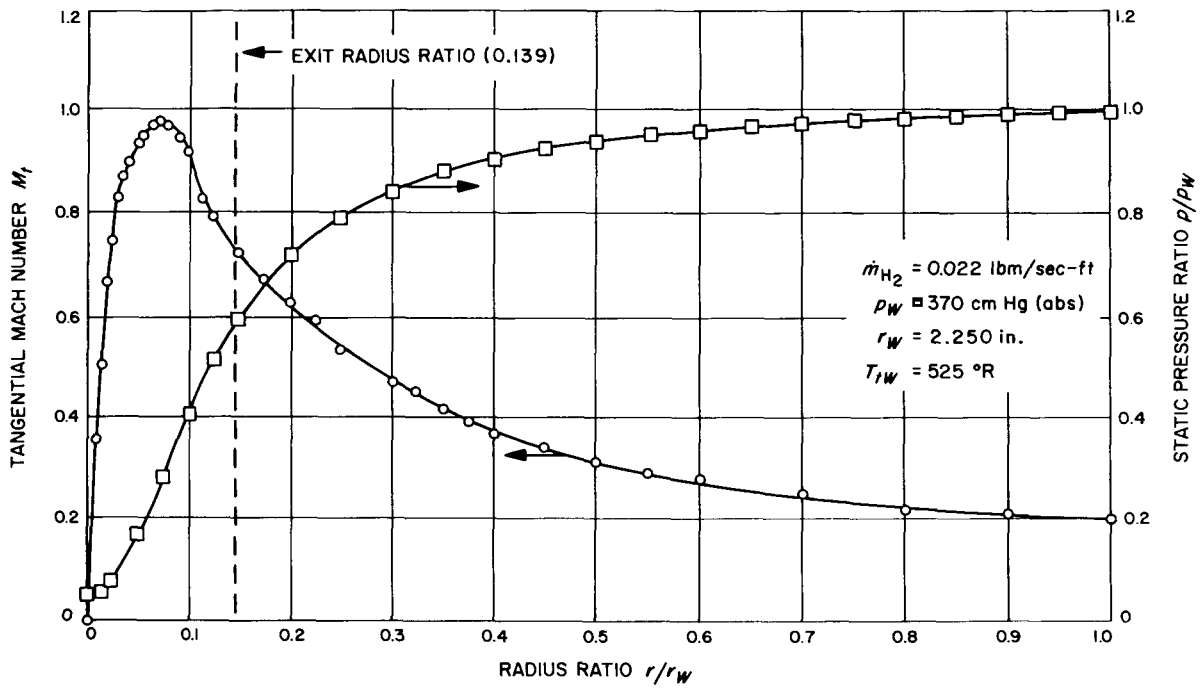

Fig. 34. Radial static pressure and tangential Mach number distributions for a high-strength vortex

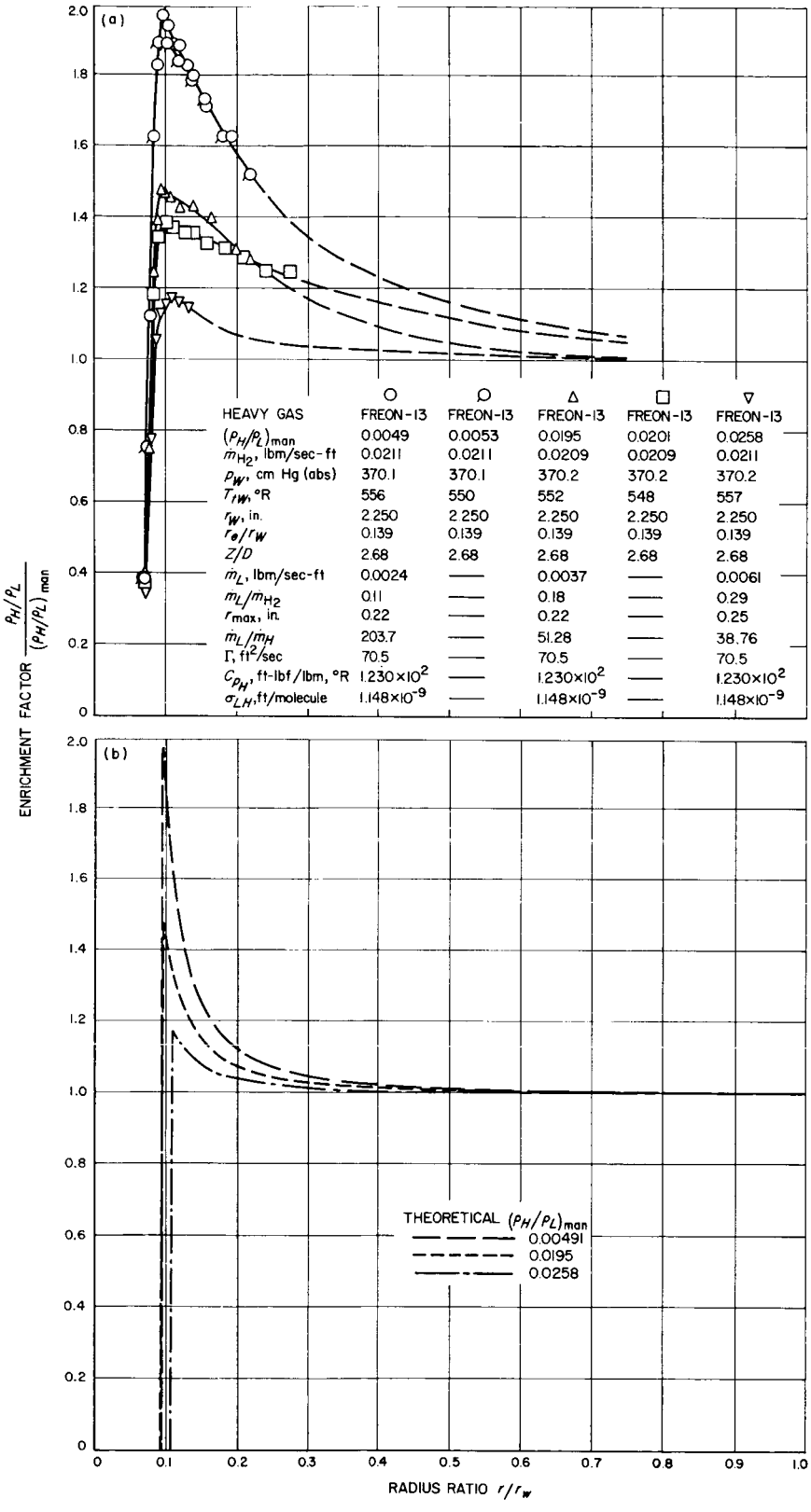

Fig. 35. Effect of Freon-13 mass flow rate on the density ratio distribution

IV. CONCLUSIONS AND SUMMARY OF RESULTS

A. Analytical Development

An analysis has been presented for a binary, two-dimensional (no axial velocities), axisymmetric, steady, compressible, potential vortex flow and a laminar diffusion process with no heat generation or chemical reactions. It was assumed that the two species would differ, at least in molecular weight, and that the flow would be radially inward. The results obtained from this analysis are:

1. The radial distribution of ρ_H/ρ_L has but one maximum and the radial location of this maximum increases as the radial light gas mass flow rate decreases. Also as this mass flow rate decreases, the distributions become broader in the vicinity of this maximum.

2. There exists a critical light gas mass flow rate with respect to achieving large maximum enrichment factors. If, for any given set of conditions, the actual radial mass flow rate is greater than this critical rate the maximum enrichment factor is modest, whereas if the mass flow rate is reduced below the critical, the maximum enrichment factor becomes very large.

3. This critical mass flow rate increases approximately as the first power of the heavy gas molecular weight and approximately as the square of the circulation, but is very nearly independent of the heavy to light gas particle flow rate ratio.

4. If the actual radial mass flow rate is less than critical, the maximum enrichment factor is approximately inversely proportional to the heavy to light gas mass flow ratio.

5. For any given set of conditions, the maximum enrichment factor increases as the heavy gas molecular weight increases.

B. End-Wall Static-Pressure Measurements

From the radial static pressure distribution on both end walls of a jet-driven vortex tube in which the fluid was extracted through an orifice at the center of one end wall, it was found that:

1. The radial pressure gradient driving potential for mass diffusion in a vortex-type flow is finite but small at the vortex periphery, rises to a maximum value very near the vortex centerline, and then decreases to zero at the centerline.

2. The maximum radial pressure gradient increases with increasing mass flow rate and with decreasing exit orifice diameter or increasing peripheral static pressure.

3. The radial location of the maximum radial pressure gradient is always inside the exit-hole radius, increases with increasing exit-hole radius, and is almost independent of mass flow rate.

4. A significant effect of the type of probe described is to decrease the maximum radial pressure gradient equally over the vortex tube length. This effect is lessened as the probe diameter is decreased, or as the tangential velocity is increased.

C. Radial and Axial Distributions of the Density Ratio ρ_H/ρ_L

From heavy to light gas mass density ratios, as measured at several axial and radial positions in a jet-driven vortex tube by withdrawing samples of the binary mixture with a probe for analysis, it was found that:

1. Although there is qualitative agreement between the experimental radial distributions of the heavy to light gas mass density ratio and the two-dimensional theory, the diffusion process is believed to be dominated by the three-dimensional aspects of the flow occurring near the vortex tube centerline.

2. The enrichment factor, defined as the density ratio divided by the heavy to light gas mass flow rate ratio, increases as the heavy gas mass flow rate decreases and as the heavy gas molecular weight is increased.

3. The radial location of the maximum density ratio is inside the exit orifice radius but outside the radius at which the radial pressure gradient reaches its maximum. The minimum density ratio was found at approximately the radius at which the radial pressure gradient reaches its maximum.

4. The nondimensional heavy gas diffusion velocity $\bar{u}_H/(D_{LH}/r_W)$ is mainly a function of the molecular weight ratio and radial pressure gradient; it is only slightly influenced by the resulting density ratio gradients.

5. The actual radial mass flow rate at the radius of maximum density ratio was found to be approximately 10% of the mass flow rate injected into the vortex tube. The radial mass average velocity at this radial location is then approximately equal to the heavy gas diffusion velocity.
6. From the limited amount of data obtained with the heavy gas injected at the center of the closed end wall, it appears that the radial distribution of the heavy gas can be tailored. In particular, it appears that a relatively large mass of heavy gas can exist near the center of the flow with very little located near the cylindrical wall. In the gaseous-vortex reactor concept, however, this tailored distribution must be coupled with a suitably low fuel loss rate, which requires a much stronger vortex than has been generated for this investigation.

At present, it is not possible to establish whether the results of the two-dimensional theory can be applied directly to the real flow. The experimental density ratio distributions agree qualitatively with the theory, however, and the maximum enrichment factor increases with decreasing mass flow rate ratio, as is predictable from the theory. This indicates that the significant diffusion processes are the same in the two flows. Therefore, there may also be a critical mass flow rate in the three-dimensional flow.

NOMENCLATURE

Symbols

- a distance from disk centerline to pressure tap, 1.063 in.
- C_0 parameter in equation for critical mass flow rate
- C_p specific heat at constant pressure
- d probe diameter
- D vortex tube diameter
- D_{LH} binary diffusion coefficient
- g_c gravitational constant
- k Boltzmann's constant
- m molecular mass
- $\dot{m}$ mass flow rate
- M_t tangential Mach number
- n particle density
- $\dot{n}$ particle flow rate
- p static pressure
- r radial coordinate
- R gas constant
- T static temperature
- u_0 mass average absolute radial velocity
- u_H heavy gas absolute radial velocity
- $\bar{u}_H$ heavy gas radial diffusion velocity (relative to u_0)
- v tangential velocity
- w axial velocity
- Z axial distance from closed end wall
- γ ratio of specific heats
- δ width of annular vortex tube exit hole
- θ angular orientation of disk
- ρ mass density; $\bar{\rho}$, average mass density
- σ_{LH} average collision diameter
- Γ constant in equation for a potential tangential velocity distribution
- ϕ angular orientation of selsyn armature

Subscripts

- c centerline
- crit critical condition
- e exit hole radius
- H heavy gas
- H_2 hydrogen gas
- L light gas
- m maximum tangential Mach number
- man vortex tube manifold
- max maximum density ratio or pressure gradient
- min minimum density ratio
- N_2 nitrogen gas
- t stagnation conditions
- W cylindrical wall
- ∞ conditions at infinite radius

REFERENCES

1. Kerrebrock, J. L., and Meghreblian, R. V., "Vortex Containment for the Gaseous-Fission Rocket," *Journal of the Aerospace Sciences,* Vol. 28, No. 9, September 1961.
2. Kendall, J. M., Jr., *Experimental Study of a Compressible Viscous Vortex,* Technical Report No. 32-290, Jet Propulsion Laboratory, Pasadena, California, June 5, 1962.
3. Rosenzweig, M. L., Ross, D. H., and Lewellen, W. S., "On Secondary Flows in Jet-Driven Vortex Tubes," *Journal of the Aerospace Sciences,* Vol. 29, No. 9, September 1962.
4. Keyes, J. J., Jr., and Dial, R. E., "An Experimental Study of Vortex Flow for Application to Gas-Phase Fission Heating," *Nuclear Rocket and Ram Jet Engines,* ORNL-2837, C-86, June 13, 1960.
5. Ragsdale, R. G., "*Applicability of Mixing Length Theory to a Turbulent Vortex System,*" NASA, TN D-1051, Lewis Research Center, Cleveland, Ohio, August 1961.
6. Iwao, S., "Exact Solutions for Ordinary Nonlinear Differential Equations," *Electrical Communication,* Vol. 37, No. 1, pp. 47–55, 1961.
7. Iwao, S., "A Class of Solved Riccati's Equations," *Electrical Communication,* Vol. 37, No. 1, pp. 56–60, 1961.
8. Pivirotto, T. J., "Radial Static Pressure Distributions in Confined Compressible Vortex Flow Fields," Jet Propulsion Laboratory, Pasadena, California (to be published).
9. Chapman, S., and Cowling, T. G., *The Mathematical Theory of Non-Uniform Gases,* Cambridge University Press, New York, 1958.
10. Rietema, K., and Krajenbrink, H. J., "Theoretical Derivation of Tangential Velocity Profiles in a Flat Vortex Chamber — Influence of Turbulences and Wall Friction," *Applied Scientific Research,* Section A, Vol. 8, 1958.
11. Brokaw, R. S., "Alignment Charts for Transport Properties Viscosity, Thermal Conductivity, and Diffusion Coefficients for Nonpolar Gases and Gas Mixture at Low Density," NASA TR R-81, Lewis Research Center, Cleveland, Ohio, 1961.